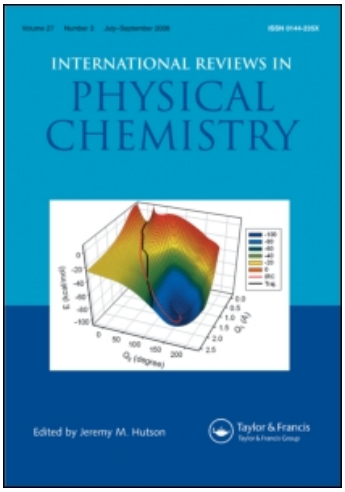

International Reviews in Physical Chemistry
Publication details, including instructions for authors and subscription information:
http://www.informaworld.com/smpp/title~content=t713724383

Four-atom bimolecular reactions with relevance in environmental chemistry: Theoretical work

A. J. C. Varandas

Online publication date: 26 November 2010

To cite this Article Varandas, A. J. C.(2000) 'Four-atom bimolecular reactions with relevance in environmental chemistry: Theoretical work', International Reviews in Physical Chemistry, 19: 2, 199 — 245
To link to this Article: DOI: 10.1080/01442350050020888
URL: http://dx.doi.org/10.1080/01442350050020888

INT. REVIEWS IN PHYSICAL CHEMISTRY, 2000, VOL. 19, NO. 2. 199–245

Four-atom bimolecular reactions with relevance in environmental chemistry: theoretical work

A. J. C. VARANDAS
Departamento de Química, Universidade de Coimbra,
P-3049 Coimbra Codex, Portugal

We review some of the work that we have been doing in the field of elementary reactive processes with interest in atmospheric chemistry and combustion processes. After a brief analysis of the relevant potential energy surfaces, we report dynamics studies of four tetratomic chemical reactions: (1) $O + O_3 \rightarrow O_2 + O_2$; (2) $H + O_3 \rightarrow O_2 + OH$; (3) $O + HO_2 \rightarrow O_2 + OH$; (4) $M + HCN \rightarrow M + H + CN$ (M is a third body). Reaction (4) as well as the reverse of reactions (1)–(3) have so far been investigated by running classical trajectories, although reactions (1)–(3) have additionally been studied by quantum-mechanical reduced-dimensionality methods. The emphasis will be on the quantum versus classical comparison, and the agreement with the available kinetics measurements.

Contents

International Reviews in Physical Chemistry ISSN 0144-235X print/ISSN 1366-591X online © 2000 Taylor & Francis Ltd
http://www.tandf.co.uk/journals

1. Introduction

The necessary starting point for the study of environmental chemistry (taken here as the study of gas-phase reactions with relevance in atmospheric chemistry and combustion processes) is not only the understanding of its general characteristics but above all the rationalization of the elementary processes that influence its composition through reactive collisions. In fact, a detailed knowledge of the properties of such collisional processes is a key element both for modelling the chemical components arising in environmental problems and for the interpretation of work with lasers. Their study is therefore vital for an understanding of many phenomena, some having practical and even social implications. Thus, it is not surprising that an explosive growth in studies of this kind has occurred in recent years.

So far as atmospheric chemistry is concerned, the processes focused in this work refer to the so-called oxygen and hydrogen families of reactions in the chemistry of ozone. They are involved in catalytic cycles of destruction of 'odd oxygen', namely

$$X + O_3 \rightarrow XO + O_2, \tag{1}$$

$$O + XO \rightarrow O_2 + X \quad (X = O, H, OH \text{ or } HO_2), \tag{2}$$

$$\text{net:} \quad O + O_3 \rightarrow 2O_2, \tag{3}$$

and we shall address the following four-atom reactions:

$$O + O_3 \rightarrow 2O_2, \tag{4}$$

$$H + O_3 \rightarrow OH + O_2, \tag{5}$$

$$O + HO_2 \rightarrow OH + O_2. \tag{6}$$

Although it is only a small part of the general reaction scheme [1] shown in figure 1, such reactions are the most influential and involve only natural species with a high abundance in the atmosphere. Given their important role in atmospheric chemistry, they have therefore been the object of extensive experimental and theoretical consideration in several laboratories including our own (references to this work will be given below in the applications). We have also reported [2, 3] on the four-atom association reactions

$$O + O_2 + M \rightarrow O_3 + M, \tag{7}$$

$$H + O_2 + M \rightarrow HO_2 + M, \tag{8}$$

which play an important role in the formation of ozone; M is a closed-shell third body. However, the present work refers only to bimolecular reactions, and hence no further reference will be made here to such recombination processes.

Although industrialized nations have devoted much attention to research studies of ozone photochemistry with a view to understanding the ozone destruction cycles

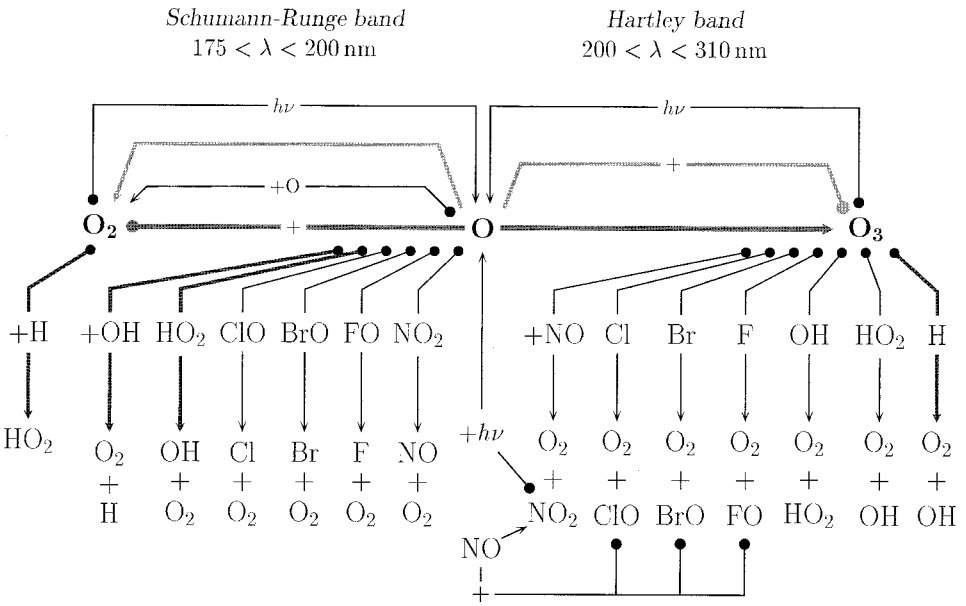

Figure 1. General scheme for reactions in the atmosphere related to production or loss of odd oxygen in the stratosphere [1]. The range of radiation bond lengths associated with photodissociation of O_2 (Schumann–Runge band system, which is associated with the absorption from the X to the B state in O_2) and O_3 (Hartley band) are also indicated. The greyish or thicker solid lines show reactions which were studied by our group.

(and hence the ways in which its loss is accelerated by human activity), interest has also arisen recently on the details of how it is created owing to the existing discrepancy between the upper atmospheric model predictions of ozone and satellite observations. Because these predictions in the region from 50 to 80 km are lower than the observations by a factor of 1.5–2 [4, 5] this issue became known as the 'ozone deficit problem' [6–9]. In fact, the standard view has been that increased ozone production could only occur through increased O_2 dissociation: the solar radiation at wavelengths shorter than 246 nm would photodissociate oxygen, and the resultant atoms form O_3 by $O + O_2$ three-body recombination [7]. Thus, ozone has for some time been viewed as a 'do-nothing' process in terms of changing the ozone balance. However, it can have a significant effect, particularly if photoabsortion rates are far larger than those for oxygen. Indeed, an alternative source of ozone has been proposed [9–12] on the basis of the reaction of vibrationally excited O_2 ($v \geqslant 26$) with ground state O_2, namely

$$O_2(X\,^3\Sigma_g^-, v' \geqslant 26) + O_2(X\,^3\Sigma_g^-, v'' = 0) \rightarrow O_3 + O(^3P). \tag{9}$$

As a source of vibrationally excited triplet oxygen, it has been suggested (for example [7] and references therein) the well known photodissociation of ozone in the Hartley band which occurs in the atmosphere through the following two spin-allowed channels:

$$O_3 + h\nu(\lambda < 243\ \text{nm}) \rightarrow O_2(a\,^1\Delta_g, v) + O(^1D) \tag{10}$$

$$\rightarrow O_2(X\,^3\Sigma_g^-, v) + O(^3P), \tag{11}$$

of which the singlet is predominant (85–90%); $h\nu$ is a photon, and h is the Planck constant. Note that the pressure is low (say a few torrs at 40 km) and hence collisional

relaxation is slow. As a result, the internal energy distribution of atmospheric constituents is expected to be far from equilibrium. We shall comment further on the above mechanism (the so-called Wodtke mechanism) in section 3.

On the combustion side, we focus on the reaction $M + HCN \rightarrow M + H + CN$, which is of relevance in propellant combustion chemistry and, more generally, in combustion of nitrogen-containing materials at high temperatures [13]; for simplicity, the closed-shell third-body species M will be taken as an argon atom. Noteworthy dissociative reactions of this type have not been considered on modelling [14] the combustion chemistry of nitrogen compounds for temperatures up to 2500 K, although the removal of HCN by dissociation is expected to be competitive with oxidation by atomic oxygen at high temperatures. Also of relevance would be the reverse association reaction [15]

$$H + CN + Ar \rightarrow HCN + Ar \tag{12}$$

which, for the above reasons, will not be discussed in the present work.

We address now the study of elementary chemical reactions which is most commonly based on two underlying assumptions. The first is the Born–Oppenheimer separation of electronic and nuclear motions, reducing the molecular dynamics to the motion of the nuclei on a single potential energy surface. The other is methodological and refers to the integration in time of the equations for the nuclear motion using classical dynamics. However, there are many chemical issues of current interest for which one or both of these underlying approximations are invalid. For example, dynamics involving light atomic nuclei such as hydrogen atoms require in principle for accuracy the use of a quantum description of the nuclear motion. Zero-point energy effects and tunnelling through reaction barriers assume then a fundamental role and can only be accurately described using the methods of quantum dynamics. Exact quantal methods are, however, unaffordable for most systems of chemical interest and hence approximate quantal approaches or mixed classical–quantum treatments are most welcome to address such issues. In this case, a strategy could be to retain a classical mechanical treatment and design fixes to account for the problem of zero-point energy leakage [16–33] while introducing tunnelling effects into the trajectory calculations (see [34–36], and references therein). On moving to further complexity, one encounters processes which involve conical intersections of potential energy surfaces such as those typically encountered on collisions between open-shell species and photoinduced chemistry, which usually occur on more than one potential energy surface with transitions among them. We shall comment on them further below.

The traditional approach to molecular dynamics is by far one which is based on the two following steps. First, the relevant potential energy surface (or surfaces) is calculated by solving the electronic Schrödinger equation for a set of fixed positions of the nuclei. The calculated electronic energies are then added to the nuclear repulsion, and the resulting potential energies fitted to some convenient analytical form, typically a single-valued function. Such a procedure is now standard and (unusual) complexity is expected to arise only when more than one electronic state of the same symmetry (i.e. a multivalued potential energy surface) must be taken into account. We have addressed this issue in a systematic way by extending to such systems the formalism previously developed for single-valued surfaces [37, 38]. The method has a sound quantum mechanical origin which stems from using diatomics-in-molecules (DIM) theory [39] as the backbone [40, 41]. The approach, known generally as the double many-body expansion (DMBE) method [37, 40, 41], can produce the complete mani-

fold of surfaces of a given symmetry for atoms of arbitrary spin and angular momentum. Indeed, the DMBE approach has yielded some of the most reliable functions currently available for well known prototype systems such as H_3 [42], Li_3 [43, 44], HO_2 [45, 46], HC_2 [47], HCN [48], O_4 [49] and HO_3 [50]. Of these, O_4 and HO_3 will be examined later in the applications.

Although economical, the traditional route to dynamics described in the previous paragraph can be cumbersome, with the modelling of the potential energy surface being non-trivial and by far the most demanding step from the viewpoint of human resources. In fact, it is to a large extent an art and as such requires special skills for being completed with success. An alternative route is 'on-the-fly dynamics' [51–53], where the potential energy surface(s) is (are) calculated as needed along the course of the nuclei motion (trajectories). Unfortunately, such an approach is viable only for classical dynamics studies and is extremely expensive owing to the accuracy requirements demanded in solving the electronic Schrödinger equation when aiming to obtain accurate simulations. Recently, we have proposed an approach which can significantly reduce the computational labour while leading to reliable potential energies, gradients and Hessians. Such a goal is achieved at the expense of introducing one scaling parameter *per* reaction channel; thus, the method has been named quasi-*ab-initio* dynamics [53]. Although showing much promise towards avoiding the analytical representation of the full potential energy surface, further exploitation of its capabilities is necessary to establish its feasibility for studies of four-atom and larger systems.

Exact quantum calculations are the ultimate goal not only because they provide the true result for a given potential energy surface but also because they serve as benchmark for testing approximate theories which are the only affordable ones for four-atom and larger polyatomic reactions. Several papers [54–61] and books [62, 63] have reviewed this field recently, and hence we focus on approximate reduced-dimensionality theories which we have been developing in the past few years [64–69] (for another review of some of these methods, see [70]).

A final comment should go to reactive processes which are influenced by non-adiabatic effects, that is the dynamical properties depend on more than one potential energy surface. This is the case whenever two or more adiabatic potential energy surfaces cross each other, giving rise to conical intersections. Well established examples of such intersections occur in H_3 [42], Li_3 [43] (in general trimers of ^2S atoms [71]) and HO_2 [46–72]. Such intersections materialize either directly or indirectly on the underlying dynamics. Direct effects arise when the trajectories (in a classical dynamics sence) sample both intersecting adiabatic potential energy surfaces. Conversely, conical intersections manifest indirectly through symmetry effects known as the geometric phase effect [73] (also called the molecular Bohm–Aharonov effect [74] or Berry's [75] phase effect) associated with the non-uniqueness of the electronic wavefunction. Such indirect effects are elusive and show up when the energy is sufficiently high to complete a loop around the point of conical intersection, that is even when the energy is considerably below its minimum value along the crossing seam. Rather than the exception, the rule in environmental chemistry is then probably the need to take into account non-adiabatic effects. Yet, most calculations carried out to date are based on the assumption of adiabaticity, and this will also be assumed to be valid here. Thus, all calculations reported in this work are based on the premise that only one electronic state is involved. Specifically, reactions (4)–(6) have been studied on global DMBE potential energy surfaces which were modelled from *ab initio*

electronic structure calculations and fine-tuned using empirical data, while, for reaction (12), we have employed a realistic potential energy surface [76] obtained from the energy switching [77, 78] (ES) method which reproduces the vibrational–rotational data of the Ar…HCN van der Waals molecule.

The plan of the paper is as follows. Section 2 presents the theory. The solution of the electronic problem is briefly summarized in section 2.1 while the problem of representing the potential energy surface is discussed in section 2.2. In turn, the theory relevant to the dynamics calculations is presented in section 2.3. Section 3 presents the results obtained for case studies. The conclusions and prospective of planned work are in section 4.

2. Theory

2.1. *The solution of the electronic problem*

The solution of the electronic Schrödinger equation is central to the use of quantum mechanics for the calculation of the potential energy surface. Of course, it is a many-body problem, and hence it is in general very cumbersome. In practice it proves only feasible to obtain approximate solutions, and it is the degree of approximation that is the crucial question.

We shall distinguish between *ab initio* and semiempirical methods for the calculation of the potential energy surface, although other researchers consider four categories in descending order of reference to theory: *ab initio*, semitheoretical (if the parametrization is based only on data obtained from *ab initio* calculations of greater accuracy), semiempirical and empirical (if the potential model has a purely arbitrary form with no reference to theory). With *ab initio* methods, one selects the appropriate model and then performs in a pointwise manner the calculation of the potential energy surface without further approximations. Thus, in the *ab initio* methods the approximation lies in the choice of the model. Of course, an unrealistic choice of this model leads to an unrealistic potential energy surface, and hence it is clear that the qualification *ab initio* does not necessarily imply accuracy being often only synonymous of very expensive.

For a given model the best choice of approximation will depend on the value of the interaction energy. In the region of weak interactions, perturbation theory is justified not only to establish the proper asymptotic functional form of the various contributions to the interaction energy but also for the direct calculation of this energy, considered as a perturbation to that of the interacting systems. Conversely, in the region of strong interactions, the most common approach is to calculate the interaction energy by subtracting the energy of the infinitely separated subsystems from the energy of the supermolecule, all energies being calculated using the variational method.

In the semiempirical approach, one therefore recognizes that it is very difficult to obtain energies which are of 'chemical accuracy' (less than 1 kcal mol^{-1}) of experiment, and hence one achieves a realistic representation of the potential energy surface through parametrization of a model Hamiltonian or a model potential energy surface. In this case theory helps in setting the analytical model (e.g. in the partition and representation of the potential energy), while its calibration is done from accurate *ab initio* energies, experimental data, or both. Therefore it is not surprising that the semiempirical methods have been by far the major source of potentials used for dynamics studies. Indeed they offer two important advantages. First, by built-in construction, they may be chosen to reproduce important topographical details which are known to play an essential role in the dynamics. Second, they usually give (an

exception is the DIM [39] method in its most general form [79, 80]) the potential energy surface in explicit form, which is an essential requirement to speed up the calculation of the potential energy and its gradient at an arbitrary geometry of the molecule configuration space.

2.2. *Potential energy surfaces*

A successful approach to the potential energy surfaces of small polyatomic molecules developed in recent years is the DMBE method [37, 38, 40, 41, 81, 82]. It provides an extension of the popular many-body expansion [83] approach and has given some of the most accurate currently available potential energy surfaces for well known prototype systems [42, 43, 45, 47, 49, 50, 84]. The DMBE method has been applied both to single-valued (see [45, 49, 50, 85–87], and references therein) and double-valued [42, 43, 47, 84, 88] potential energy surfaces and has more recently [40, 41, 46] been developed to provide a general strategy to deal with multivalued potential energy surfaces for interacting atoms with any spin multiplicity and angular momentum.

Although there is a clear understanding that non-adiabatic effects are of increasing concern, single-valued potential energy surfaces will continue to be of utmost interest in the years to come. Thus, there is a great demand for single-valued potential energy surfaces even for the simplest triatomic systems. Here, we focus on the DMBE formalism for single-valued functions, although not entering into details which the reader can find elsewhere [37, 38, 41].

As we have pointed out earlier, one appealing feature of DIM theory is its quantum-mechanical origin. The central feature of DIM consists of partitioning the electronic Hamiltonian $\mathscr{H}$ into diatomic and monatomic parts as follows:

$$\mathscr{H} = \sum_K \sum_{L>K} \mathscr{H}^{KL} - (N-2) \sum_K \mathscr{H}^K, \tag{13}$$

where the atomic Hamiltonian operator $\mathscr{H}^K$ depends on the electrons and coordinates of atom K, and $\mathscr{H}^{KL}$ depends on the electrons and coordinates of atoms K and L and their interactions. The term $N-2$ corrects for the multiple counting of the atomic fragments. If used in a pure *ab initio* form, DIM can lead in principle to the exact solution of the electronic problem. However, it has been as a semiempirical theory that it has afforded its greatest popularity. The remarkable advantage then is that it preserves the correct structure of the potential matrix, while leading to significant computational savings by avoiding the explicit calculation of molecular integrals. To achieve such a goal in a practical way, however, one generally needs to use minimal basis sets and to ignore overlap between the basis functions. Unfortunately, this is accurate only in the case of a complete set of diatomic basis functions. Thus, in real applications with finite basis sets, the DIM matrix elements lack many-centre terms. Although it appears that polyatomic potential energies are largely independent of whether or not overlap between basis functions is included, we may additionally wish to compensate for such neglect of orbital overlap. We have recently shown [41] how to introduce such many-body correction terms and yet preserve the structure of the DIM potential matrix. One obtains for the diatomic matrix

$$\mathbf{H}^{AB} = \mathbf{R}^{AB}\mathbf{T}^{AB}\mathbf{E}^{AB}(\mathbf{1} + \mathbf{F}^{AB})\mathbf{T}^{AB\dagger}\mathbf{R}^{AB\dagger}, \tag{14}$$

where $\mathbf{R}^{AB}$ is a direct product of the rotation matrices (these rotate the A_i and B_j eigenvectors so that their z axes are aligned with the internuclear axis of diatomic AB), $\mathbf{T}^{AB}$ is a spin-recoupling matrix which transforms the original coupling of the spin

states to a coupling in which A couples with B, and $\mathbf{F}^{AB}$ is a matrix of *ad hoc* many-body 'dressing functions' which contain adjustable parameters; corresponding expressions apply for the other diatomic matrices. Of course, the DIM expression is recovered if we consider $\mathbf{F}^{AB} = \mathbf{0}$.

Consider now the simplest case of interacting ^{1}S atoms. Because the rotation and spin matrices are now 1×1 unit matrices, the resulting single-valued potential surface assumes the pairwise additive form

$$E(\mathbf{X}^N) = \sum_{\mathbf{X}^2 \subset \mathbf{X}^N} E^{(2)}(\mathbf{X}^2)[1 + F^{(N)}(\mathbf{X}^N)], \tag{15}$$

where $\mathbf{X}^n$ specifies any set of $n(n-1)/2$ interatomic distances referring to n atoms, which is a subset of $\mathbf{X}^N \equiv (X_1, X_2, \ldots, X_{N(N-1)/2})$, and the energies of the isolated atoms have been taken as the reference energy; $N(N-1)/2 \geqslant 3N-6$. Clearly, the dressing functions $F^{(N)}$ account for many-body interactions higher than two-body interactions. Thus, the pure DIM result would simply be the sum of the three undressed diatomic potential energy curves.

For convenience, we partition now the potential energy into an extended Hartree–Fock part (indicated by subscript EHF) and a dynamical correlation part (indicated by subscript dc). Without any loss of generality, we may further develop the $(n > 2)$-body energies $E^{(2)}_{\mathrm{EHF}}F^{(N)}$ and $E^{(2)}_{\mathrm{dc}}F^{(N)}$ in the form of a cluster expansion. The result is

$$E(\mathbf{X}^N) = \sum_{n=2}^{N} \sum_{\mathbf{X}^n \subset \mathbf{X}^N} [E^{(n)}_{\mathrm{EHF}}(\mathbf{X}^n) + E^{(n)}_{\mathrm{dc}}(\mathbf{X}^n)], \tag{16}$$

which is the familiar double many-body expansion for single-valued potential energy surfaces. It is therefore clear that the use of equation (16) to represent the potential energy surface of interacting atoms of any spin state and angular momentum rests on the complete neglect of the spin-recoupling and orientational effects which are inherent to the system. For open-shell atoms, chemical bonding may occur to form stable diatomic fragments, and hence there will be a deep minimum if the cluster expansion is truncated at the two-body level. To cancel such a minimum partly or totally in the case of a triatomic potential energy surface, one therefore requires the addition of a strongly repulsive three-body energy term. Similarly, other important attributes of the potential energy surface such as crossings and avoid crossings will, of course, be absent. Not surprisingly therefore, equation (16) may in some cases be a poor starting point for an accurate fit of the complete adiabatic potential energy surface. For such cases, a more appropriate treatment consists of diagonalizing the potential matrix that results from equations (13) and (14).

Ideally, a global potential energy surface should be capable of achieving spectroscopic accuracy at regions where that information is available. Recently, we have proposed such a method which is based on the switching between two forms: the global form V_1, which provides a realistic although not necessarily accurate description of the surface at all regions of configuration space; the other local form V_2, which is capable of achieving spectroscopic accuracy near the minima to which the available spectroscopic information pertains. Because the switching from one function to the other uses the energy as criterion, the method has been called energy switching (ES) [77]. Thus, the ES potential energy surface assumes the form

$$V_{\mathrm{ES}} = f(\Delta E)\, V_1(\mathbf{R}) + [1 - f(\Delta E)]\, V_2(\mathbf{R}), \tag{17}$$

where $\Delta E = E - E_0$ is the displacement from some reference energy, $\mathbf{R} \equiv \mathbf{X}^3$, and f is

a switching function that approaches zero for large negative energy displacements and becomes +1 for large positive energy displacements. A convenient form for f may be

$$f = \tfrac{1}{2}\{1 + \tanh[\gamma(\Delta E)\,\Delta E]\}, \tag{18}$$

where γ is a function of E containing disposable parameters to be defined from other criteria. As prototype systems, the ES method has been extensively tested on the water molecule for which single-value [77], double-valued [78] and triple-valued [89] global potential energy surface (of DMBE-type quality) have been completed which reproduce the vibrational spectroscopy of H_2O to within a few reciprocal centimetres. Similar applications have been reported by other workers, for example for H_3^+ [90]. Another class of system for which the ES method has revealed itself particularly useful are polyatomic van der Waals molecules such as ArHCN [76]. This system will be discussed in some detail in section 3.

2.3. *Reaction dynamics*

2.3.1. *Arrangement channels and coordinate systems*

One of the challenges in the theory of reaction dynamics for systems with more than three atoms is on the rapidly growing number of ways that atoms can group together to make molecules. In fact, there are three arrangement channels for a triatom reactive process while the number increases to 14 in the tetratomic case: three diatom–diatom and 11 atom–triatom channels. This number may indeed be larger if one counts as distinct arrangements those which correspond to different isomeric species (e.g. HCN and HNC). As a result, there are compounded difficulties to describing the involved kinematics and dynamics, starting with the choice of coordinates as described next.

The most common and general coordinate system is Cartesian. If Cartesian coordinates are employed, the classical Hamiltonian of a general N-atom system assumes the form

$$H = \sum_{i=1}^{N} \frac{\mathbf{p}_i \cdot \mathbf{p}_i}{2m_i} + V(\mathbf{x}_1, \ldots, \mathbf{x}_N) \tag{19}$$

where $\mathbf{x}_i$ and $\mathbf{p}_i$ are the positions (shown in the upper parts of figure 2) and momenta respectively of the ith atom, m_i is the mass of the ith atom and V is the potential energy. From the Hamiltonian function, one may write the corresponding quantum-mechanical Hamiltonian operator using the well established rules of quantum mechanics. Examples of such Hamiltonian operators will be given later in section 2.3.3, and hence we omit them here.

Since the potential energy depends only on the relative positions of the atoms but not on the position of the centre of mass, the potential is quite often written in terms of internal distances. The specific choice of these coordinates depends on the problem at hand. It follows that the number of differential equations to be integrated is reduced by six, although chain rule terms appear when determining the derivatives with respect to the new coordinates. Figure 2 illustrates the possible situations which arise in the four-particle ABCD problem when one assumes that one diatom bond (CD) remains inert (this corresponds to the assumption made in the quantum-dynamical models which are discussed below; for a similar assumption, see [59]). Thus, there are two possible atom–triatom arrangement channels (A + BCD and B + ACD, of which only the former is illustrated in figure 2), and a diatom–diatom channel (AB + CD).

Consider then the A + BCD case. We may define the coordinates such that

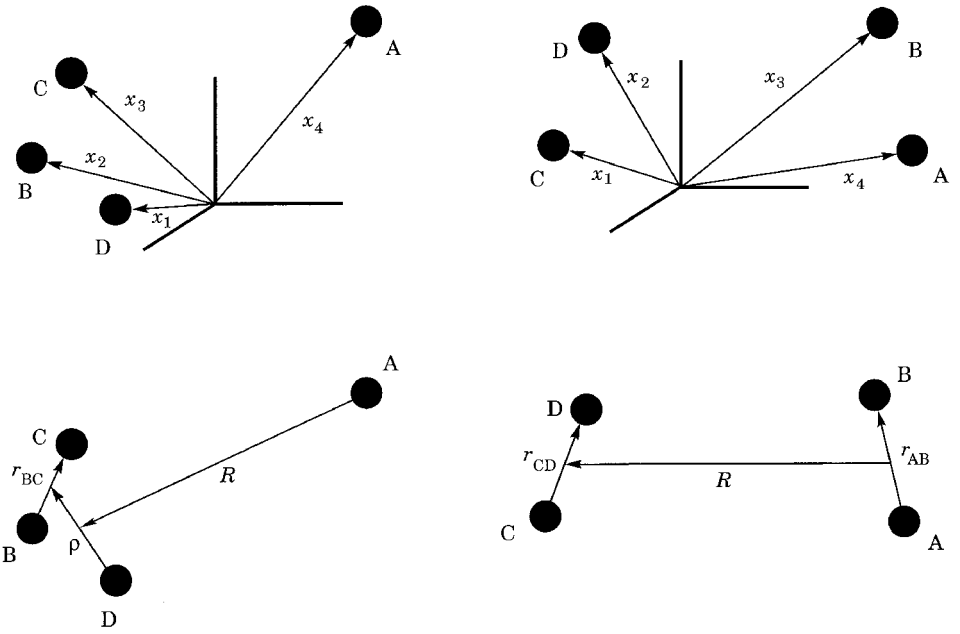

Figure 2. Atom–triatom and diatom–diatom Jacobi coordinate systems: (*a*) A + BCD; (*b*) AB + CD.

x_i ($i = 1$–3) are the coordinates of atom A relative to those of the centre of mass of BCD (with coordinates x_j ($j = 10$–12)), x_j($j = 4$–6) are the coordinates of B relative to C, and x_j ($j = 7$–9) those of D relative to the centre of mass of BC. These are the so-called Jacobi coordinates for the A + BCD arrangement channel. The classical Hamiltonian for the relative motion assumes then the form

$$H = \frac{1}{2\mu_{\mathrm{A,BCD}}}\sum_{j=1}^{3} p_j^2 + \frac{1}{2\mu_{\mathrm{B,C}}}\sum_{j=4}^{6} p_j^2 + \frac{1}{2\mu_{\mathrm{D,BC}}}\sum_{j=7}^{9} p_j^2 + V(x_1, \ldots, x_9), \tag{20}$$

where p_j are the conjugate momenta of x_j, V is the interaction potential energy surface (which does not vary with the position of the centre of mass of the four-atom system), and the reduced masses are defined as follows:

$$\mu_{\mathrm{A,BCD}} = \frac{m_{\mathrm{A}}(m_{\mathrm{B}} + m_{\mathrm{C}} + m_{\mathrm{D}})}{m_{\mathrm{A}} + m_{\mathrm{B}} + m_{\mathrm{C}} + m_{\mathrm{D}}}, \tag{21}$$

$$\mu_{\mathrm{B,C}} = \frac{m_{\mathrm{B}} m_{\mathrm{C}}}{m_{\mathrm{B}} + m_{\mathrm{C}}}, \tag{22}$$

$$\mu_{\mathrm{D,BC}} = \frac{m_{\mathrm{D}}(m_{\mathrm{B}} + m_{\mathrm{C}})}{m_{\mathrm{B}} + m_{\mathrm{C}} + m_{\mathrm{D}}}. \tag{23}$$

Similarly, to treat the diatom–diatom case, we may choose the Jacobi coordinates displayed in figure 2(*b*). The Hamiltonian becomes

$$H = \frac{\mathbf{p}_{r\mathrm{AB}} \cdot \mathbf{p}_{r\mathrm{AB}}}{2\mu_{\mathrm{A,B}}} + \frac{\mathbf{p}_{r\mathrm{C_D}} \cdot \mathbf{p}_{r\mathrm{C_D}}}{2\mu_{\mathrm{C,D}}} + \frac{\mathbf{p}_R \cdot \mathbf{p}_R}{2\mu_{\mathrm{AB,C_D}}} + V(x_1, \ldots, x_9), \tag{24}$$

where

$$\mu_{A,B} = \frac{m_A m_B}{m_A + m_B}, \tag{25}$$

$$\mu_{C,D} = \frac{m_C m_D}{m_C + m_D}, \tag{26}$$

$$\mu_{AB,CD} = \frac{(m_A + m_B)(m_C + m_D)}{m_A + m_B + m_C + m_D}. \tag{27}$$

Note that, in both cases, three Jacobi angles complete the description of the system; these are not indicated in figure 2 and will be defined later for specific applications. Thus, in equations (20) and (24), we have chosen to define the potential energy surface in terms of the nine Cartesian coordinates. Again, the new coordinates are most appropriate for the diatom–diatom case but, as we have seen in the previous paragraph, rather less useful when describing the product channel if the outcome is an atom plus a triatom. Of course, Cartesian coordinates are as appropriate as before, although the Jacobi coordinates are quite convenient for visualization purposes. Indeed, the choice of coordinates plays a crucial role in quantum mechanics, although it is far less important in classical mechanics. In general, it is worthwhile using Jacobi coordinates for three-atom and four-atom systems.

2.3.2. *Classical trajectory method*

The classical trajectory method is now a standard tool [91] in reaction dynamics (for example [92, 93], and references therein) and hence we give here only the essential details by focusing on the four-atom case. If full three dimensions are employed, one has in Cartesian coordinates $\mathbf{x}_i = (x_i, y_i, z_i)$ and $\mathbf{p}_i = (p_{x_i}, p_{y_i}, p_{z_i})$, with the positions and momenta satisfying Hamilton's equations

$$\dot{\mathbf{x}}_i = \frac{p_i}{m_i}, \tag{28}$$

$$\dot{\mathbf{p}}_i = \nabla_i V. \tag{29}$$

Given the coordinates and momenta at some instant of time, one can then obtain their values at some future instant by numerically integrating equations (28) and (29) to simulate the collisional process. Frequently (especially in the atom–diatom case), the reagent molecules are given initial coordinates and momenta which correspond to the semiclassical eigenstates being studied. Similarly, the states of the product molecules can be assigned by determining the good actions that determine the vibrational–rotational motion of the product molecules. They are then rounded to the nearest integer multiple of $\hbar$ to define the corresponding quantum states. Thus, the approach is known as the quasiclassical trajectory method (QCT). Clearly, there are numerous difficulties when one goes beyond the triatom case. First, the calculation of the vibrational actions for polyatomics (more than two atoms) is far from trivial and involves non-standard calculations if one aims at accurate results. Second, the vibrational and rotational actions are well defined only if the molecular motion is quasiperiodic. These difficulties have been reviewed elsewhere [60], and the reader is referred to this reference and those cited therein for details. Perhaps more important here is to stress that QCT methods suffer from the omission of tunnelling and zero-point energy leakage. Progress has recently been made [34–36] towards the goal of

introducing multidimensional tunnelling into trajectory calculations but its usefulness in tetratomic molecules has not yet been tested. While the absence of tunnelling effects is expected to be important at threshold and subthreshold energies, zero-point energy leakage can in general introduce important errors. Two types of fix have been suggested for this problem. The simplest approaches, called 'non-active' methods, consist of throwing out the trajectories (both reactive and non-reactive) which exhibit unphysical product energies [18, 20, 21]. However, the number of reactive trajectories is typically less than the number of unreactive trajectories, and hence the method tends to decrease the number of trajectories sampled from the reactive part of the initial phase space. Such a procedure can be improved by weighting of the trajectories sampled in the reactive and non-reactive portions of phase space [24]. In the 'active' methods, a constraint is introduced into the dynamics which prevents the trajectories of entering the region of phase space which would allow the vibrational modes to have less than its zero-point energy [16, 17, 22, 23, 25–33]. Unfortunately, none of the two approaches is free from some ambiguity, which makes this topic an interesting issue awaiting future developments.

There are other non-trivial issues which need to be addressed when running trajectories for a tetratomic system, in particular how to set the initial conditions, and how to partition the energy in the products. They are discussed in several excellent reviews [92, 93], to which the reader is referred for details. In the remainder of this section we then focus on the extraction of observables such as cross-sections and rate constants from them.

Let N^{r} be the number of reactive trajectories out of a total of N trajectories sampled. The cross-section is then approximately given by

$$\sigma^{\mathrm{r}} = \pi b_{\max}^2 \, P^{\mathrm{r}}, \tag{30}$$

where $b_{\max}$ is the maximum impact parameter which leads to reaction, and $P^{\mathrm{r}} = N^{\mathrm{r}}/N$ is the reactive probability. In turn, the standard deviation in the cross-section is given by

$$\Delta\sigma^{\mathrm{r}} = \sigma^{\mathrm{r}} \left(\frac{N - N^{\mathrm{r}}}{N N^{\mathrm{r}}} \right)^{1/2}. \tag{31}$$

If a sufficiently large number of trajectories is run, then the differential cross-section (i.e. the product attribute scanned in the scattering angle θ_{scatt} between the initial vector and the centre of mass velocity vector of some fragment of interest) may also be calculated as

$$\frac{\mathrm{d}^2\sigma(\theta)}{\mathrm{d}\omega^2} = \frac{\pi b_{\max}^2 \, P^{\mathrm{r}}(\theta)}{2\pi \sin\theta}, \tag{32}$$

with the angle variable being binned according to the usual procedure.

Finally, rate constants can be obtained by Monte Carlo sampling the initial energies for a canonical distribution or by calculating cross-sections at several translational energies E_{tr} and then calculate the following integral:

$$k(T) = g \left(\frac{2}{k_{\mathrm{B}} T} \right)^{3/2} \frac{1}{(\pi \mu^{1/2})} \int_0^\infty E_{\mathrm{tr}} \sigma^{\mathrm{r}}(E_{\mathrm{tr}}) \exp\left(\frac{-E_{\mathrm{tr}}}{k_{\mathrm{B}} T} \right) \mathrm{d}E_{\mathrm{tr}}, \tag{33}$$

where μ is the reduced mass of the reactants and g is the appropriate electronic degeneracy factor which represents the probability that a given collision occurs on the considered potential energy surface; k_{B} is the Boltzmann constant.

2.3.3. *Reduced-dimensionality quantum-dynamical methods*

Except for the simplest triatomic and tetratomic systems involving light atoms such as $H + H_2$ and its isotopomers [94–98], $F + H_2$ and its isotopomers [99–103], $O + H_2$ [104], $Cl + H_2$ [105], other atom–diatom reactions [106], H_2 (D_2) + OH [107–110] and H_2 (D_2) + CN [111, 112], the quantum treatment of four-atom (and larger polyatomic) reactions which have practical interest has at present to be carried out within some approximation. Perhaps even more rarely [113], quantum dynamics studies on tetratomic reactions involved more than one potential energy surface. However, affordable reduced-dimensionality schemes have been suggested to treat four-atom and eventually larger polyatomic systems by Bowman and Wang [59], Clary [61, 114], and Balakrishnan and Billing [115]. Since these and more exact calculations have been reviewed by Bowman and Schatz [60], we focus here on the methods that we have recently developed with Szichman and Baer [64, 65, 68, 69]. These have been successfully applied to reactions of practical interest, which will be described in section 3.

The methodology involves three basic steps:

(*a*) use of a perturbative-type Schrödinger equation to treat non-reactive collisions in a given arrangement channel

$$(E - H)\,\Psi_\lambda = 0, \tag{34}$$

where H is the full Hamiltonian for the motion of the nuclei, and Ψ_λ is the total nuclear wavefunction which is expanded in terms of a short-range wave function χ_λ and the asymptotic incoming component ψ_λ, that is $\Psi_\lambda = \chi_\lambda + \psi_\lambda$;

(*b*) conversion of equation (34), which treats non-reactive processes, into an equation for treating reactive processes by adding to H negative imaginary potentials (NIPs) [116] such as to decouple the reactive arrangement channels and to allow the use of L^2 basis sets to expand the local vibrational modes;

(*c*) conversion of the scattering problem into a bound-type problem by introducing an additional NIP in the λ (reagents) asymptotic region, which enables use of the R-propagation method for also expanding χ in a bound translational space.

The aim of the method is therefore to calculate all non-reactive probabilities, that is $\mathbf{P}(\lambda \leftarrow \lambda_0)$ the sum of which is then subtracted from unity to obtain the total reactive probability. Thus,

$$P_r^J = 1 - \sum_\lambda |S^J(\lambda \leftarrow \lambda_0)|^2, \tag{35}$$

where

$$S^J(\lambda \leftarrow \lambda_0) = \left(\delta_{\lambda\lambda_0} + \frac{1}{i\hbar}\langle \psi_\lambda | V | (\chi_{\lambda_0} + \psi_{\lambda_0})\rangle\right) \exp(i\phi_\lambda), \tag{36}$$

with $\delta_{\lambda\lambda_0}$ being the Kronecker delta function and ϕ_λ the (elastic) λth phase shift (see appendix A). In equation (36), $S^J(\lambda \leftarrow \lambda_0)$ is an element of the non-reactive scattering $\mathbf{S}^J$ matrix, and λ (and λ_0) stands for a set of quantum numbers which labels the reagent four-atom system. If $\tilde{\mathbf{S}}$ is the reactive transition matrix, $\mathbf{S}^J$ can also be written as [117, 118]

$$\mathbf{S}^J = \mathbf{I} - \tilde{\mathbf{S}}^J, \tag{37}$$

where $\mathbf{I}$ is the unity matrix; for the one-dimensional case, equation (37) is equivalent to equation (36) since in this case the phase shift in $\tilde{\mathbf{S}}^J$ is π.

Prior to the calculation of the **S**-matrix terms, the following Schrödinger equations must therefore be solved:

$$(E-H)\chi_\lambda = V_\lambda \psi_\lambda \tag{38}$$

and

$$(E-H_0)\psi_\lambda = 0, \tag{39}$$

where V_λ is the λ-perturbative potential and ψ_λ represents the λth quantum-mechanical solution of the unperturbed (elastic) Schrödinger equation. Assuming the unperturbed solution for the initial state ψ_{λ_0} to be known, the full solution Ψ_λ may then be written as

$$\Psi_{\lambda_0} = \psi_{\lambda_0} + \chi_{\lambda_0}, \tag{40}$$

where it can be easily shown that χ_{λ_0} can be obtained by solving the inhomogeneous Schrödinger equation (38) in the close interaction region. Thus, H_0 is the unperturbed Hamiltonian which describes the atom–triatom system, and $V_\lambda = H - H_0$, with NIPs being *ad hoc* added to H. These are defined along the boundaries of the arrangement channel in which ψ_{λ_0} is calculated, and assume usually the linear ramp form [116, 119]

$$U_{\mathrm{I}}(r) = \begin{cases} -iU_{0\mathrm{I}}\dfrac{r-r_0}{\Delta r}, & r_0 \leqslant r \leqslant r_0 + \Delta r, \\ 0, & \text{otherwise}, \end{cases} \tag{41}$$

where the height $\Delta U_{0\mathrm{I}}$ of the NIP and its width Δr are chosen in such a way as to ensure that reflection will be negligibly small; the value of r_0 is chosen large enough to ensure that the NIP does not interfere in the process taking place in the strong interaction region.

For the calculations in an atom–triatom configuration, the Jacobi coordinate system shown in figure 2 is commonly employed. Thus, the atom–triatom (reagent) channel is described by three radial distances and three Jacobi angles. The former include the vibrational coordinate for the unbroken bond r, the corresponding 'translational' coordinate ρ of the triatom connecting the third atom with the centre of mass of the unbroken bond, and the translational coordinate R which connects the fourth atom to the centre of mass of the triatomic system. Three Jacobi angles complete the description of the system: θ (the angle between r and ρ); γ (the angle between ρ and R); β (the polar angle between the triatom plane and R).

Within a four-dimensional infinite-order sudden approximation (IOSA) approach, ψ_{λ_0} (and χ_{λ_0}) can be calculated using [120]

$$H = -\frac{\hbar^2}{2mr}\frac{\partial^2}{\partial r^2}r - \frac{\hbar^2}{2\mu\rho}\frac{\partial^2}{\partial\rho^2}\rho - \frac{\hbar^2}{2MR}\frac{\partial^2}{\partial R^2}R + \left(\frac{1}{2\mu\rho^2}+\frac{1}{2mr^2}\right)\mathbf{j}^2 + \left(\frac{1}{2\mu\rho^2}+\frac{1}{2MR^2}\right)\mathbf{K}^2 + \frac{\hbar^2 J(J+1)}{2MR^2} + U(r\rho R\theta\gamma|\beta), \tag{42}$$

where $\mathbf{j}$ and $\mathbf{K}$ represent the bending and rotational angular momentum operators respectively of the triatomic molecule. In turn, m, μ and M denote in an obvious correspondence the reduced masses of the diatomic bond, triatomic molecule and atom–triatom system. Note that equation (42) is the result of applying the close-coupled states (or j_z) [121, 122] approximation to a more general expression for H [66, 120]. Note also that an averaged potential energy surface (see later) may be used instead of U.

The Schrödinger equation which follows by employing the Hamiltonian defined in equation (42) is then treated twice: once to calculate the asymptotic (unperturbed) elastic wave function ψ_{λ_0}, and a second time to calculate χ_{λ_0}. Consider first the expression for the (unperturbed) potential energy surface used to calculate ψ_λ in equation (39). One has

$$U(r\rho R\theta|\beta) = v(r\rho\theta) + w(R|\beta), \tag{43}$$

where $v(r\rho\theta)$ is the potential energy surface of the triatomic molecule,

$$v(r\rho\theta) = \lim_{R\to\infty}[U(r\rho R\theta\gamma\beta)], \tag{44}$$

while the distortion potential $w(R|\beta)$ may be defined as an eigenvalue of the following rotational Schrödinger equation:

$$\left[\left(\frac{1}{2\mu\rho_e^2}+\frac{1}{2MR^2}\right)\mathbf{K}^2 + U(r_e\,\rho_e\,R\theta_e\,\gamma|\beta) - w(R|\beta)\right]h(R\gamma|\beta) = 0, \tag{45}$$

with ρ_e, r_e and θ_e being the equilibrium properties [123] of the triatomic molecule, and β an IOSA angle [64, 66, 124].

In a three-dimensionality treatment where the angular directions are fixed, $(\mathbf{K},\mathbf{K}) \equiv 0$, and hence equation (45) leads to

$$w(R|\beta) = U(r_e\,\rho_e\,R\theta_e\,\gamma|\beta). \tag{46}$$

To eliminate the dependence of w in β and γ, we may take β as a fixed (IOSA) parameter or use the five-dimensional polar-averaged potential energy surface

$$\bar{U}(r\rho R\theta\gamma) = \frac{1}{\pi}\int_0^\pi U(r\rho R\theta\gamma\beta)\,\mathrm{d}\beta. \tag{47}$$

Note that, in IOSA, γ is taken as a fixed parameter or instead U is averaged using $\cos\gamma$ over the range $(0,\pi)$ [106, 120]. Such an averaging is equivalent to weighting the potential with the lowest-order spherical harmonics $y_{0,0}(\gamma|\beta)$, although it would be rather more realistic to use $h(R\gamma|\beta)$ for the weighting procedure. Since $h(R\gamma|\beta)$ is an undulating function which has maxima where U has minima, a simpler procedure [68, 69] consists in finding, at each value of R, the minimum of U in the range $0 \leqslant \gamma \leqslant \pi$. One is then led to introduce the angle γ_{MP} as the value of γ which minimizes $U(Rr_e\,\rho_e\,\theta_e\gamma|\beta)$. In practice, it is determined by imposing the condition of extremum

$$\frac{\partial}{\partial\gamma}U(Rr_e\,\rho_e\,\theta_e\,\gamma|\beta)|_{\gamma=\gamma_{MP}} = 0 \tag{48}$$

Thus, the method has been called the elastic optimum angle adiabatic multiple-path (EOAAMP) method [68, 69] (referred to in the text simply as MP). According to it, one may imagine the process happening so slowly that, at any translational distance R, the triatomic molecule accommodates itself within a given range of β values to the angle γ that minimizes the potential energy surface. Thus, it is in a certain sense, an approach opposite to IOSA and may *a priori* be considered to give the uppermost limit of the quantum-mechanical reactivity in a three-dimensional treatment. Similarly, one may define an elastic optimum angle adiabatic single path (EOAASP) (referred to in the text simply as SP) method in which γ_{SP} is obtained and $\bar{U}$ used instead of U in equation (48).

The function χ_{λ_0} is derived by solving equation (38) in the reagents arrangement channel. For this purpose the range of the reagents vibrational coordinate(s) are enlarged so as to comprise the relevant reactive regions and to include the necessary decoupling NIPs. Note that there is usually one preferred open channel [67, 125], and hence one may assume one of the bonds in the triatomic as remaining unbroken through the whole reactive process. To account for this, two negative imaginary terms are added to the real Hamiltonian: a vibrational term along ρ and another translational term along R, namely

$$V_I(r, \rho, R) = -\,\mathrm{i}[v_{I_\rho}(\rho) + v_{I_R}(R)]. \tag{49}$$

As already pointed out, the addition of the NIPs to U converts the scattering problem into a bound-state problem, and hence makes χ_{λ_0} expandable in terms of square integrable L^2 functions [126, 127]. These are chosen as localized functions for the translational components, and adiabatic basis sets for the vibrational components. Thus,

$$\chi^J_{\lambda_0}(r\rho R\theta\gamma|j) = \frac{1}{r\rho R}\sum_{n\lambda} a^J_{n\lambda}\, g(R|n) f(r\rho\theta\gamma|j|n\lambda), \tag{50}$$

where $g(R|n)$ represents the translational component which is chosen to be a standard Gaussian function of the form

$$g(R|n) = \left(\frac{\alpha}{\sigma\sqrt{\pi^{1/2}}}\right)^{1/2} \exp\left[-\frac{\alpha^2}{2}\left(\frac{R-R_n}{\sigma}\right)^2\right], \tag{51}$$

with $\sigma = R_n - R_{n-1}$ being the translational step size, and $f(r\rho\theta\gamma|j|n\lambda)$ an eigenfunction of the three-dimensional Schrödinger equation

$$\left[-\frac{\hbar^2}{2mr}\frac{\partial^2}{\partial r^2}r - \frac{\hbar^2}{2\mu\rho}\frac{\partial^2}{\partial\rho^2}\rho + \left(\frac{1}{2mr^2}+\frac{1}{2\mu\rho^2}\right)\mathbf{j}^2 + U(r\rho R_n\,\theta\gamma|\beta) - \varepsilon(\lambda|\theta\gamma j|R_n)\right] \times f(r\rho\theta\gamma|j|n\lambda) = 0. \tag{52}$$

Once this has been solved, it is possible to obtain the non-reactive **S**-matrix elements. From these, the reactive probabilities may then be calculated as

$$P^J_r(E_{tr}, \lambda_0) = \frac{1}{2}\int_{-1}^{1} |S^J(\lambda \leftarrow \lambda_0)|_\gamma^2\, \mathrm{d}(\cos\gamma), \tag{53}$$

while the total reactive cross-section for the triatomic ground-rotational state ($K = 0$) is given by

$$\sigma^r(E_{tr}, \lambda_0) = \frac{\pi}{k^2(E_{tr})}\sum_J (2J+1)\, P^J_r(E_{tr}, \lambda_0), \tag{54}$$

where $k(E_{tr})$ is the atom–triatom wavenumber, $k^2(E_{tr}) = (2M/\hbar^2)\,E_{tr}$ and P^J_r is the reactive probability which is calculated for each integer value of J by means of equation (35).

3. Applications

3.1. *The $O + O_3$ reaction and its reverse*

3.1.1. *The O_4 potential energy surface*

The relevant potential energy surface for studying the title reaction is that of O_4 (^{3}A) since, in C_s symmetry, the reactants O_2 ($X\,^3\Sigma_g^-$) + O_2($X\,^3\Sigma_g^-$) in nonplanar and planar geometries yield surfaces of ^{1,3,5}A″ and ^{1,3,5}A′ symmetries, while the O_3

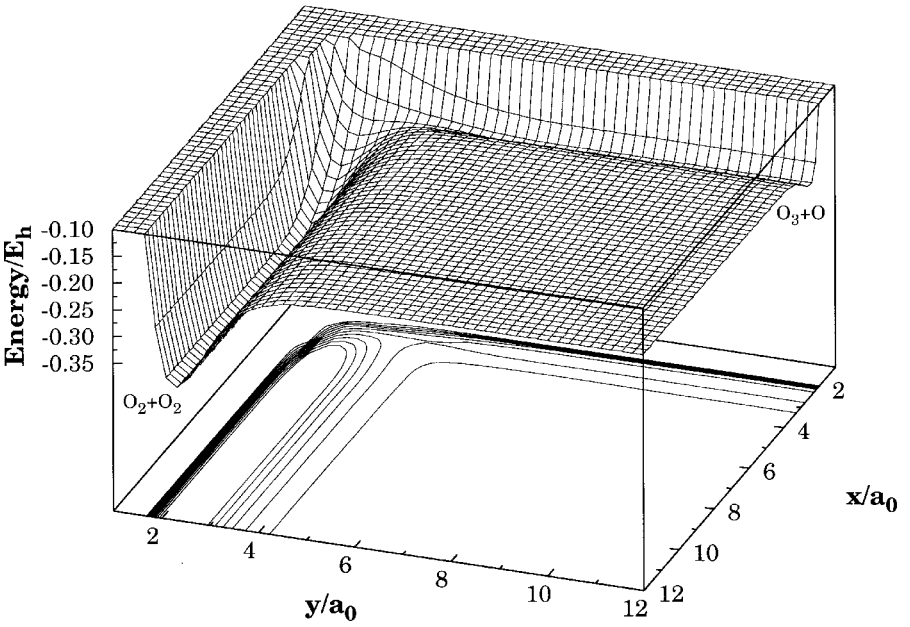

Figure 3. Perspective view for the reaction $O + O_3 \rightarrow O_2 + O_2$ considered to be in plane. x denotes the distance between the attacking oxygen atom and the terminal oxygen atom of an equilibrium ozone molecule. In turn, y is the distance between the attacked oxygen atom of ozone and the middle one.

($^1A_1$) + O (^3P) products yield one of $^3A'$ symmetry and two of $^3A''$ symmetry. Of course, the reaction with reactants in a triplet state and products in a singlet state is possible through an intersystem spin crossing. However, such a spin-forbidden transition is very unlikely, and hence may be ignored. We focus our survey below on a global potential energy surface obtained [49] within the framework of the DMBE [37, 128] method, and which has been based on a multiproperty fit including spectroscopic, dynamical and *ab initio* information.

Figure 3 shows a perspective view of this DMBE potential energy surface for the reaction $O + O_3 \rightarrow O_2 + O_2$. The notable features are the small barrier separating the reactants from the products and the high exoergicity of the reaction leading to two oxygen molecules. Such features are best seen in figure 4 which shows the corresponding minimum-energy path. Also indicated are the energies associated to various vibrational combinations of the two oxygen molecules. Clearly, the exoergicity is enough to produce combinations with one molecule vibrationally excited as high as $v = 27$.

In figure 5 is shown a perspective view relevant for the reverse endoergic reaction, that is for ozone formation starting from two O_2 molecules. Specifically, the O_4 DMBE potential energy surface is shown for a partially relaxed O_2 moving around another partially relaxed O_2 which lies along the x axis with the centre of mass fixed at the origin. Visible from this plot is a small minimum corresponding to a structure of T_d symmetry. Note that it lies below the saddle-point energy ($E = 97.96$ kcal mol^{-1} relative to $O_2 + O_2$) for the $O + O_3$ reaction and represents a kind of four-atom analogue for the known metastable cyclic (D_{3h}) structure of ozone. To our knowledge, there is no *ab initio* data to support such a prediction. However, there exists some evidence from *ab initio* calculations for the presence of a minimum below the $O + O_3$

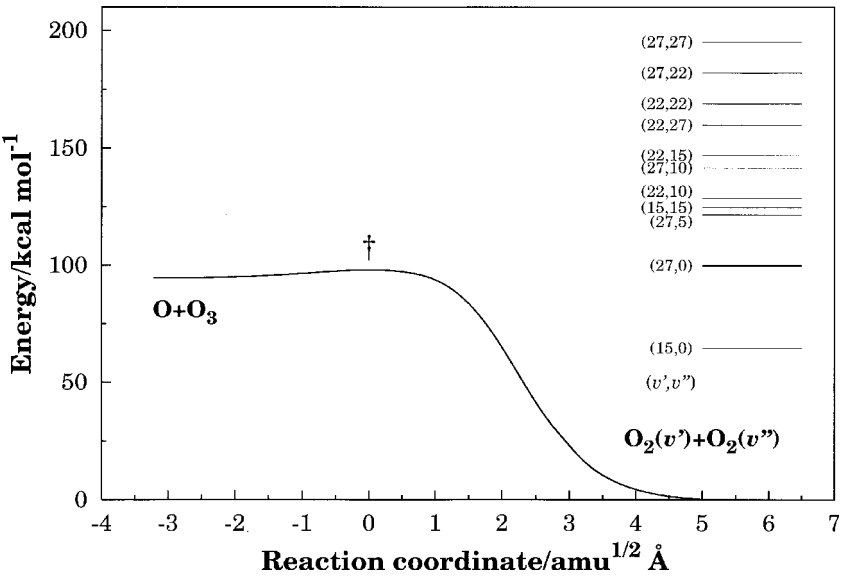

Figure 4. Minimum-energy path for the reaction $O + O_3 \rightarrow O_2 + O_2$. Also shown are the energies associated with various vibrational combinations of the resultant oxygen molecules. The dark line indicates the combination (27, 0) which lies just above the classical threshold for the reverse endothermic reaction.

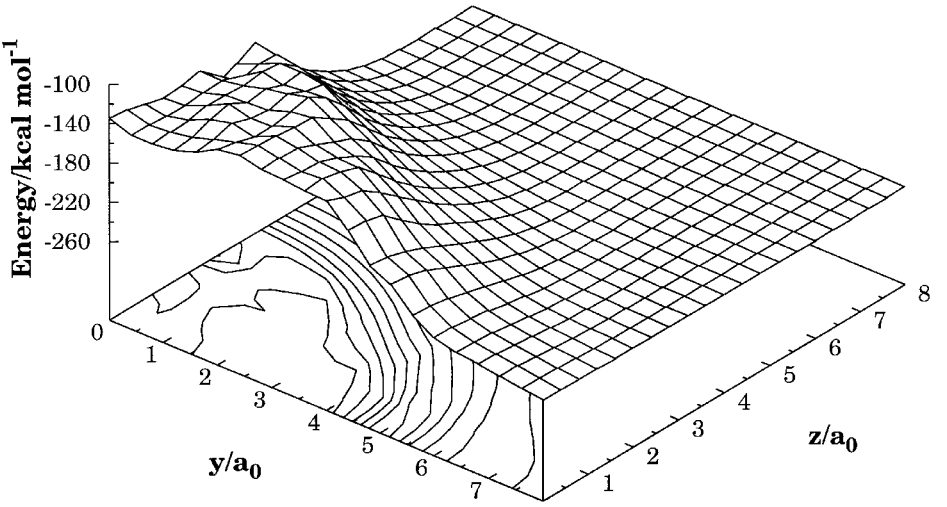

Figure 5. Perspective view relevant for the endoergic reaction $O_2 + O_2 \rightarrow O_3 + O$. The potential energy surface is shown for a partially relaxed O_2 molecule moving around another partially relaxed O_2 molecule which lies along the x axis with the centre of mass fixed at the origin. The shallow minimum which is visible in the high-energy region at ($y = 0$, $z \approx 2.5a_0$) corresponds to a tetrahedral O_4 structure (it corresponds to a minimum on the potential energy surface which has not yet been confirmed through reliable *ab initio* calculations).

products energy in the potential energy surface for the single state of O_4. Such evidence led Mack *et al.* [129] to postulate the existence of an equivalent minimum on the triplet state surface with a view to rationalizing their own measurements for the $O + O_3$ reaction. Apparently, such an assumption did not encounter support on recent

Table 1. Geometry and energy of transition state[a] for the reaction $O + O_3 \rightarrow O_2 + O_2$

	DMBE [49]	CASSCF [130]	MRCI [130]
R_{ab} (units of a_0)	2.416	2.368	
R_{bc} (units of a_0)	2.514	2.605	
R_{cd} (units of a_0)	4.214	3.771	
$\theta_{O_aO_bO_c}$ (degrees)	117.6	111.4	
$\theta_{O_bO_cO_d}$ (degrees)	139.6	104.1	
$\phi_{O_aO_bO_cO_d}$ (degrees)	118.2	86.3	
Energy[b] (kcal mol^{-1})	97.9	48.7[c]	56.9[d], 98.8[e]

[a] The oxygen atoms are labelled by lower-case letters, for example R_{ab} is the bond distance for O_aO_b. In turn, $\theta_{O_aO_bO_c}$ and $\theta_{O_bO_cO_d}$ are the angles between O_aO_b and O_bO_c, and O_bO_c and O_cO_d respectively, while $\phi_{O_aO_bO_cO_d}$ is the dihedral angle.

[b] Relative to $O_2 + O_2$.

[c] Optimized from complete-active-space self-consistent-field calculations which included six molecular orbitals sharing only six electrons, that is CASSCF (6, 6).

[d] Calculated at the MRCI level, leaving uncorrelated the first 13 molecular orbitals.

[e] Calculated at the MRCI level, leaving uncorrelated the first four molecular orbitals (the four core orbitals of the oxygen atom).

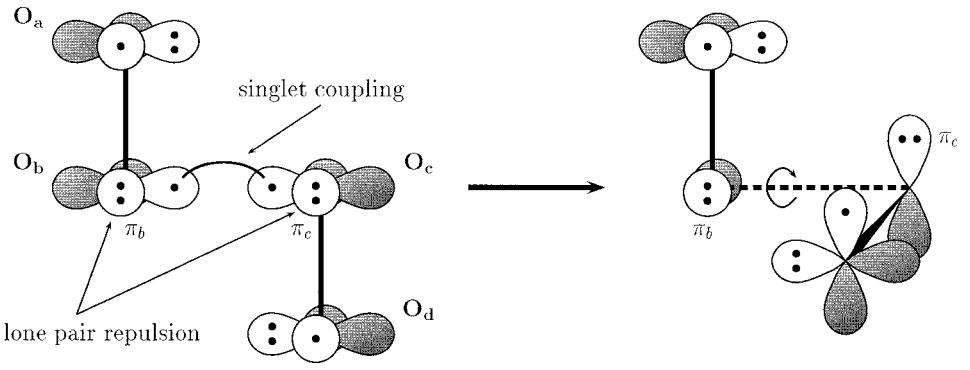

Figure 6. Valence-bond rationalization [130] of the transition state structure of O_4 as viewed from the two major interactions for the coupling of two oxygen molecules: singlet coupling of two unpaired electrons and repulsion of the π_b and π_c lone pairs.

internally contracted multireference configuration interaction (MRCI) calculations carried out by Lauvergnat and Clary [130]. These *ab initio* calculations employed large (triple-zeta-type) basis sets and accounted for some dynamical correlation. Yet, given the size of the problem at stake, only the left–right type of correlation of the two active bonds could be made with reasonable computational expense. Labelling the atoms by lower-case letters as in figure 6, such bonds have bond lengths R_{bc}, the bond length of the forming diatomic bond, and R_{cd} the bond length of the breaking bond; $\theta_{O_aO_bO_c} = \angle O_aO_bO_c$, $\theta_{O_bO_cO_d} = \angle O_bO_cO_d$ and $\phi_{O_aO_bO_cO_d}$ is the dihedral angle. Such computational limitations were then ameliorated through scaling of the computed O_4 MRCI energies using more accurate calculations or experimental data on the fragments.

Table 1 compares the geometry of the transition state predicted from the O_4

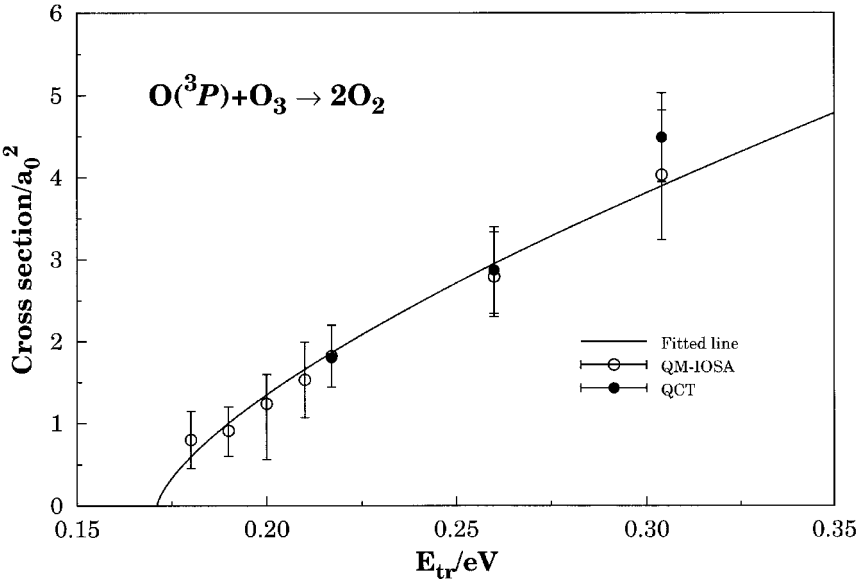

Figure 7. Cross-sections for the $O + O_3$ reaction as functions of the translational energy: (○), quantum mechanical (QM) [64, 65]; (●), classical [49].

DMBE potential energy surface with the internally contracted MRCI calculations of Lauvergnat and Clary [130]. First, we recall that the calculated transition state geometry may be rationalized using simple valence-bond theory [130]. According to this, $\theta_{O_aO_bO_c}$ and $\theta_{O_bO_cO_d}$ should be close to 90° so as to maximize overlap between the two singly occupied 2p orbitals. Similarly, the optimum value of the dihedral angle should be near 90° to minimize lone-pair repulsion between the π orbitals located on atoms b and c. Such values are not too far away from the *ab initio* values reported in table 1 but deviate slightly more from those predicted by the DMBE potential energy surface. Indeed, the agreement observed in table 1 may be considered to be good. Of course, differences exist between the MRCI calculations and DMBE predictions, especially concerning the bond angles (about 32–35° for both $\theta_{O_bO_cO_d}$ and $\phi_{O_aO_bO_cO_d}$) and bond distances (about 0.23 Å for R_{cd}). However, this is not surprising if one has in mind that the O_4 DMBE potential energy surface was not based on any *ab initio* calculations for the $O + O_3$ reaction, which were in any case unavailable at the date when it was suggested.

3.1.2. *The reaction $O + O_3 \rightarrow O_2 + O_2$*

As usual, the quantum-mechanical study of this reaction involved two steps. First, the coupled-states approximation has been employed to treat the asymptotic wavefunction ψ_λ. Then, the perturbed part of the total wavefunction was calculated using the IOSA method, often called the quasi-breathing-sphere approximation. Figure 7 compares the calculated quantum-mechanical integral cross-sections [65] as a function of translational energy with the corresponding classical values [49]. The corresponding rate constants are illustrated in figure 8 and have been obtained by fitting first the cross-sections to the form

$$\sigma(E_{tr}) = \begin{cases} C(E_{tr} - E_{tr}^0)\exp[-\beta(E_{tr} - E_{tr}^0)], & E_{tr} \geqslant E_{tr}^0, \\ 0, & E_{tr} < E_{tr}^0, \end{cases} \tag{55}$$

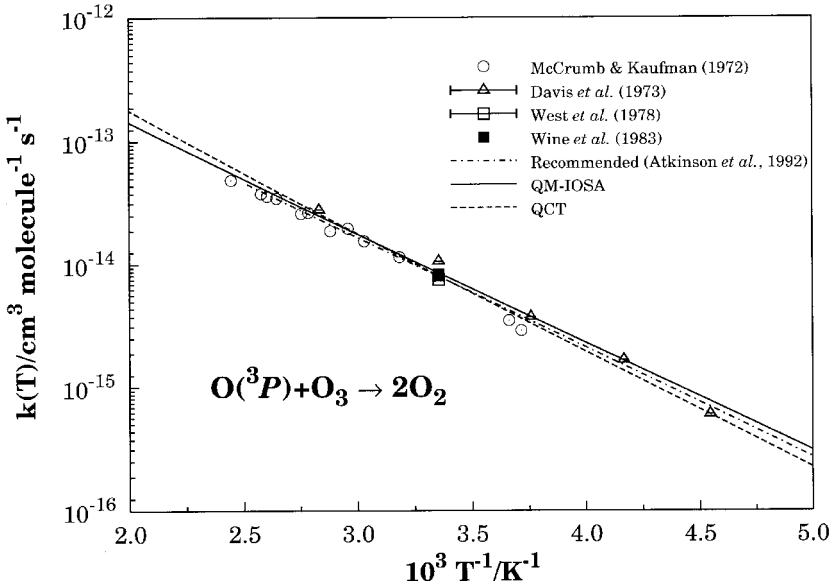

Figure 8. Rate constants for the $O + O_3$ reaction as a function of temperature: (——), quantum mechanical (QM) [64, 65]; (-----), classical [49]. Also shown are the experimental results from four groups [131–134] and the reaction rate constant (-·-) recommended by the IUPAC Subcommittee on Gas Kinetics Data Evaluation for Atmospheric Chemistry [135].

where C, n, β and E_{tr}^0 are adjustable parameters. Also presented in figure 8 are the experimental results obtained by four different groups [131–134]. The agreement between the quantum and classical values is notable as might be expected from the fact that we are dealing with heavy atoms. In turn, the good agreement with experiment suggests that the potential energy surface should be reliable in describing the kinetics of the reaction $O + O_3 \rightarrow O_2 + O_2$.

3.1.3. *The reaction* $O_2(v') + O_2(v'') \rightarrow O + O_3$

The reaction of vibrationally excited $O_2(v \geqslant 26)$ with ground-state O_2 has been proposed [9–11] as a source of ozone to explain the so-called 'ozone deficit problem' according to mechanism (9). The source of vibrationally excited triplet oxygen was suggested to be the two spin-allowed channels (10) and (11), of which the triplet channel contributes with 10–15%. In relation to reaction (11), the Wodtke and Houston groups [9–11, 136] observed, using photofragment imaging to measure the O (^3P_j) translational energy spectrum, that in the ozone photolysis at $\lambda = 226$ nm the reaction leading to O_2 (v) has a bimodal vibrational distribution peaking at $v = 14$ and 27. Such an observation has been confirmed by Syage [131] from photofragment angle–velocity distributions of the O ($^3P_{j=0,1,2}$) state in a time-of-flight spectrometer, who found also the fraction of $O_2(v \geqslant 26)$ relative to total $O_2(v)$ to be in agreement with the value of 0.08 reported by Miller *et al.* [9]; such values correspond to a quantum yield for production of $O_2(v \geqslant 26)$ of about 1%. In addition, experimental work by Stranges *et al.* [138] at 193 nm has shown the production of vibrationally excited triplet O_2 but with the vibrational distribution peaking at $v = 19$; the excited O_2 yield is in this case about 7%.

The mechanism proposed to explain the 'ozone deficit problem' (the Wodtke mechanism) involves three steps [136]:

(*a*) conjecture based on indirect kinetic measurements that the highly vibrationally excited O_2 produced in the dissociation can react with unexcited O_2 to give $O_3 + O$ [11];
(*b*) realization that the dissociation and reaction provide an autocatalytic mechanism for the production of ozone;
(*c*) observation that each ozone molecule in the stratosphere is dissociated several hundred times during its chemical lifetime, so that the autocatalytic reaction is amplified by a large factor.

Thus, each photodissociation consumes one ozone molecule but produces three. In fact, each photodissociated O_3 produces an oxygen atom and a vibrationally excited O_2; this may react with O_2 to give $O_3 + O$, while under stratospheric conditions each atom can recombine with O_2 to give ozone through an association reaction involving a third body. It should be pointed out that the modelled addition to stratospheric ozone concentrations predicted by the Wodtke mechanism has the right magnitude (an increase of up to 10% in ozone concentration over that predicted without it), although it fails to predict the correct altitude dependence to ameliorate the 'ozone deficit problem'; its effect is maximum at the lower part of the deficit region whereas the discrepancy is largest at higher altitudes [6]. This has been attributed [136] to the assumption that the yield of the newly discovered channel is constant as a function of the dissociation wavelength in the energetically permitted spectral region. It turns out, however, that an atmospheric model based on a wavelength-dependent yield [139] gives similar O_3 increases.

Figure 9 shows the results of trajectory rate constant calculations [140, 141] carried out for this reaction using the O_4 DMBE potential energy surface [49] under the assumption that the vibrational distribution of O_2 was the bimodal distribution obtained from the photofragment imaging experiments referred to above [9–11, 136]. Specifically, figure 9(*a*) presents the results for formation of both stable ozone and vibrationally excited ozone (O_3^*), while 9(*b*) and (*c*) refer to direct dissociation into $O_2 + O + O$ and oxygen-atom exchange respectively. It should be noted [140, 141] that the vibrationally resolved rate constants vary drastically with the vibrational combination of the reactant molecules but not so much with their initial rotational excitation. Yet, figure 9 shows that rotational excitation is responsible for marked differences in the temperature dependence of the vibrationally averaged rate constant for O_3^* formation. Moreover, it inhibits the dissociation reaction by a factor of 20–40% over the range of temperatures studied. However, the most controversial result is perhaps the fact that virtually no reactivity is observed [140] for the (26,0) combination originally proposed to explain the 'ozone deficit problem', a result which is in agreement with that obtained by Balakrishnan and Billing [142] using the O_4 DMBE surface and the semiclassical wave-packet method. A similar conclusion has been drawn by Hernández-Lamoneda *et al.* [143] using quantum time-dependent and time-independent methods on the same potential energy surface. Such a negative conclusion was also reached by Lauvergnat and Clary [130] who employed a scaled two-dimensional potential energy surface based on their own MRCI energies. They found that the calculated rate constants for the $O_2\ (v' = 0) + O_2(v'')$ reaction were much smaller than the experimental values even for $v'' = 26$ where reaction has been expected [10]. In another recent investigation, Campos-Martínez *et al.* [144] corroborated the same negative result by using a two-dimensional model Hamiltonian and the O_4 DMBE potential energy surface. However, if other populated vibrational

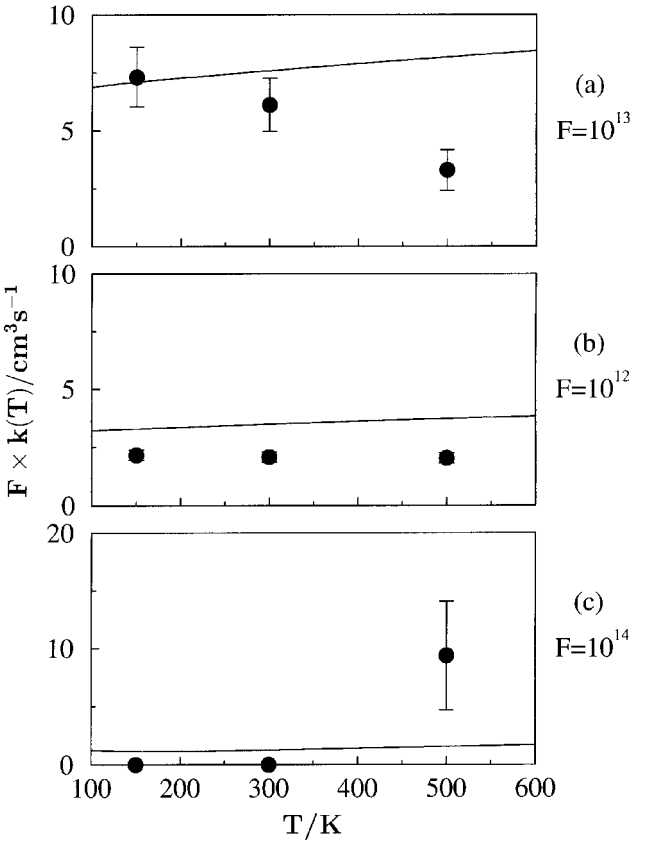

Figure 9. Calculated [140, 141] rate constants $Fk(T)$ for the $O_2(v') + O_2(v'')$ reaction under the assumption that the vibrational distribution of O_2 was the bimodal distribution obtained from the photofragment imaging experiments: (*a*) $O_2(v') + O_2(v'') \rightarrow O_3 + O$ and $O_2(v') + O_2(v'') \rightarrow O_3^* + O$; (*b*) $O_2(v') + O_2(v'') \rightarrow O_2 + O + O$; (*c*) $O_2(v') + O_2(v'') \rightarrow O_2 + O_2$. (—) Reactant molecules in their ground rotational state ($j' = j'' = 1$); ● results for the rotationally averaged rate constant. Also indicated are the error margins (these are contained within the size of the dots in (*b*)), and the appropriate F factors.

states of O_2 formed from photodissociated O_3 at 226 nm are included, the predicted vibrationally averaged rate constant [140, 141] for reaction becomes of the order of magnitude of the indirect estimates suggested from the pump–probe experiments [9, 10, 145, 146]. Clearly, this mechanism must rely on the assumption of non-local thermodynamic equilibrium (non-LTE) to increase the probability of bringing together two vibrationally hot oxygen molecules to react. Indeed, such a non-LTE equilibrium has been recognized [145] as taking place in such regions of the atmosphere. Moreover, other sources of vibrationally excited oxygen molecules may be invoked in the stratosphere besides equation (11), namely $O + HO_2 \rightarrow OH + O_2(v)$. Thus, it has been suggested [140, 141] that the title reaction should in any case be taken into account for explaining the 'ozone deficit problem'.

3.2. *The $H + O_3$, $O + HO_2$ and reverse reactions*

3.2.1. *The HO_3 potential energy surface*

As hydrogen trioxides are pivotal intermediates in atmospheric chemistry and combustion processes as well as in chemical and biological oxidation, they have been

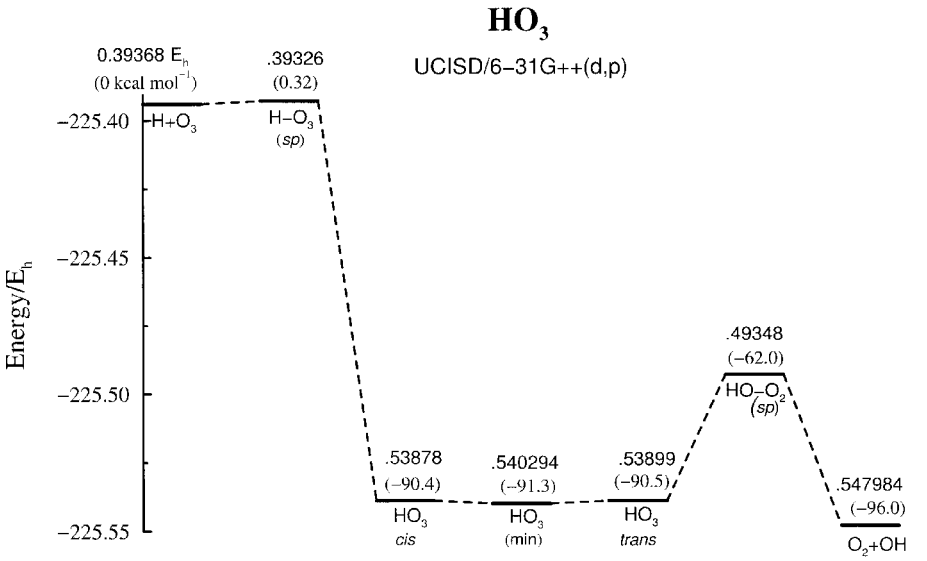

Figure 10. Schematic diagram showing the energetics of the $H + O_3$ reaction as determined from the UCISD *ab initio* calculations [50]. The numbers over the horizontal lines indicate the calculated energies once subtracted from $-225\ E_h$. In parentheses are the corresponding values in kilocalories per mole referred to the energy of the reactants. Also indicated is the nature of the relevant stationary points.

the subject of considerable theoretical [50, 142–153] and experimental [154, 155] activity. Experimentally, it has been concluded from heats of formation measured by Fourier transform ion cyclotron resonance mass spectrometry that $H_{298}^{\circ}(HOOO) = -1 \pm 5$ kcal mol^{-1}. According to this work, it is predicted [154, 155] that the title hydrogen trioxide should be a relatively stable intermediate species, lying 10 ± 5 kcal mol^{-1} below the $HO + O_2$ dissociation limit. Except for one *ab initio* prediction [151], all other theoretical estimates suggest a smaller stability. In fact, most theoretical calculations predict HO_3 to be a metastable species, which may even lie above the $HO + O_2$ dissociation limit, being separated from the products by a small activation barrier. This is the case for the HO_3 DMBE potential energy surface [50], which is employed for the calculations reported in this and the next sections. According to this DMBE surface, the lowest-energy HO_3 structure is predicted to be about 2.3 kcal mol^{-1} above the $HO + O_2$ dissociation limit, with the dissociation preceeding via a loose $HO \cdots O_2$ transition structure involving a very small activation energy. In fact, although many *ab initio* calculations were reported [50, 147–152] it is the only known global potential function which is available for the title system. It was calibrated at short range from *ab initio* unrestricted configuration interaction energies with single-electron and double-electron excitations (UCISD), while its long-range part includes the electrostatic energy up to four-body terms and the dynamic correlation energy truncated at the three-body level. Figure 10 shows schematically the energetics of the $H + O_3$ reaction as determined from the UCISD *ab initio* calculations, while the major topographical features of the HO_3 DMBE potential energy surface (this fits the calculated UCISD energies with a rms error of 2 kcal mol^{-1}) will be discussed next.

Figure 11 presents a perspective view for a H atom moving in a coplanar manner around a partially relaxed ozone molecule. Note that the positions of the oxygen

Table 2. Geometry and energy of transition state for the reaction $H + O_3 \rightarrow OH + O_2$: MC (DZP), Monte Carlo (double zeta potential).

	DMBE [49]	MC(DZP) [151]
R_{HO_a} (units of a_0)	4.4276	3.9157
$R_{O_aO_b}$ (units of a_0)	2.3850	2.4963
$R_{O_bO_c}$ (units of a_0)	2.3893	3.4801
$\theta_{HO_aO_b}$ (degrees)	112.7	107.3
$\theta_{O_aO_bO_c}$ (degrees)	114.6	112.7
$\theta_{HO_aO_bO_c}$ (degrees)	0	84.8
Energy[a] (kcal mol^{-1})	0.2[b]	2.7

[a] Relative to $H + O_3$.
[b] Relative to the bottom of the $H \cdots O_3$ van der Waals minimum; see the text.

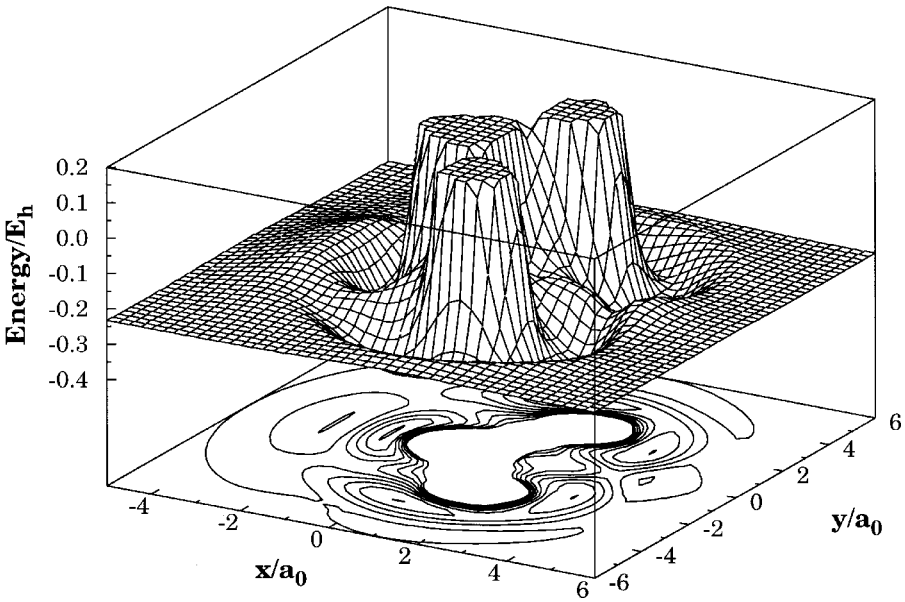

Figure 11. Perspective view for a hydrogen atom moving in a coplanar manner around a partially relaxed ozone molecule. Note that the positions of the oxygen atoms are associated with the three high central plateau regions. Thus, the middle oxygen atom is fixed at the origin while the OO bond and the $\angle$OOO have been partially relaxed (1.24 Å $\leqslant R_{OO} \leqslant$ 1.43 Å and 106° $\leqslant \angle$OOO $\leqslant$ 126°).

atoms are associated with the three high central plateau regions. Thus, the middle oxygen atom is fixed at the origin while the OO bond and the angle $\angle$OOO have been partially relaxed (1.24 Å $\leqslant R_{OO} \leqslant$ 1.43 Å and 106° $\leqslant \angle$OOO $\leqslant$ 126°). Note the three distinct stationary points (which appear as minima for planar HO_3), each associated with one of the following transition states: *cis*, HO_3; *trans*, HO_3; c_{2v}, HO_3. For the energetics, see figure 10. Clearly, there are significant orientational effects in the H–O_3 interaction. For example, a very high barrier must be overcome for reaction to take place when the hydrogen atom attacks the central oxygen atom of the ozone molecule. Such a barrier is considerably reduced for attacking angles close to the H–O bond-breaking direction in HO_3; at equilibrium, this species has a C_1 geometry characterized

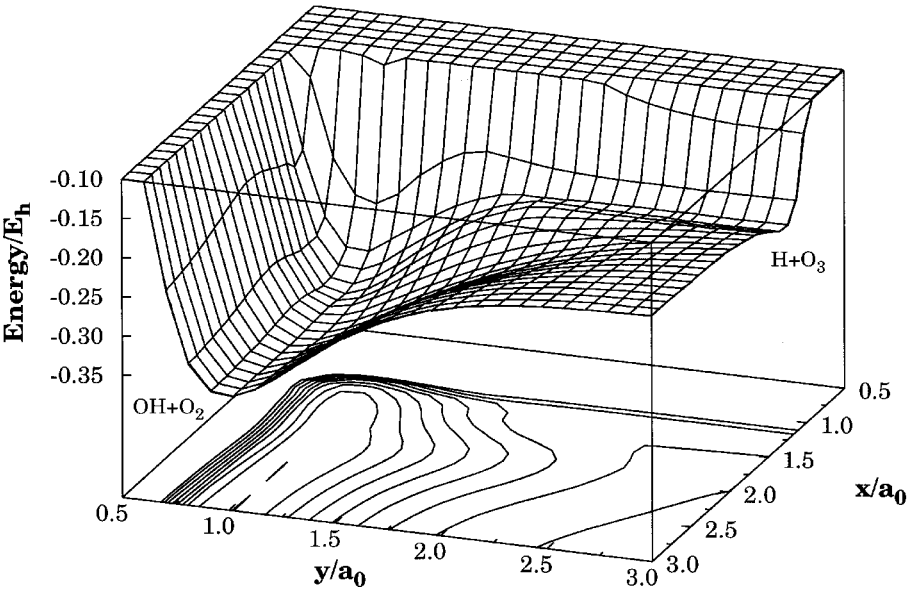

Figure 12. Perspective view of a bond-stretching plot for the reaction $H + O_3 \rightarrow OH + O_2$; x denotes the distance between the approaching hydrogen atom and the terminal oxygen atom of ozone, while y is the distance between the latter and the middle oxygen atom of O_3.

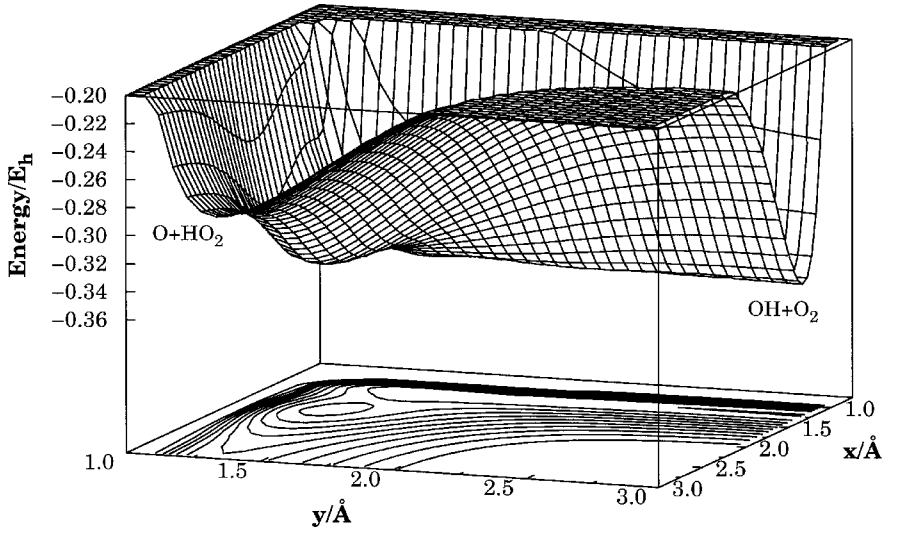

Figure 13. Perspective view of a bond-stretching plot for the reaction $O + HO_2 \rightarrow OH + O_2$ considered to be in plane; x denotes the distance between the approaching oxygen atom and the terminal oxygen atom of the hydroperoxyl radical, while y is the distance between the latter and the other oxygen atom of HO_2.

by $R_{HO_a} = 1.0035$ Å, $R_{O_aO_b} = 1.5582$ Å, $R_{O_bO_c} = 1.2336$ Å, $\theta_{HO_aO_b} = 96.2°$, $\theta_{O_aO_bO_c} = 113.5°$ and $\phi_{HO_aO_bO_c} = 90.6°$ (this is the dihedral angle). Moreover, the barrier for hydrogen attacking a terminal oxygen atom of equilibrium O_3 is lowest for an out-of-plane approach, which implies that the HO_3 DMBE potential energy surface would favour a nonlinear HO_aO_b structure for the saddle point for reaction. However, the

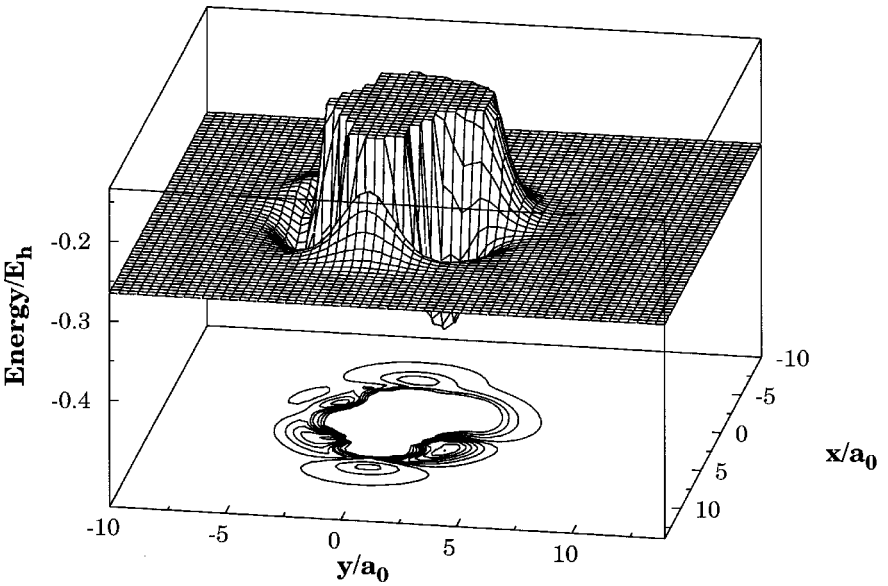

Figure 14. Perspective view for an oxygen atom moving in a coplanar manner around an equilibrium HO_2 molecule. Visible are the two minima associated with the terminal oxygen atom of the HO_2 radical (*trans* and *cis* structures), and one in the vicinity of its central oxygen atom.

barrier on the full potential energy surface is coplanar with a height of 0.2 kcal mol^{-1} relative to the H $\cdots$ O_3 van der Waals minimum but below the H + O_3 asymptote (table 2). Such a prediction finds no support on the *ab initio* multiconfiguration Hartree–Fock MC(DZP) calculations of Dupuis *et al.* [151] and our UCISD [50] calculations. Indeed, by analogy with figure 6, simple valence-bond theory would predict $\theta_{HO_aO_b} = \theta_{O_aO_bO_c} = \phi_{HO_aO_bO_c} = 90°$. Moreover, as might then be anticipated, the bond angles calculated from the MC(DZP) calculations [151] for the saddle-point geometry of the H + O_3 reaction show a striking similarity to those predicted [130] for O + O_3. Not visible from the plot in figure 11 is the small barrier discussed in the previous paragraph, which appears in the exit channel between the minimum corresponding to HO_3 and the HO + O_2 asymptote. Such a barrier can be seen in figure 12 which shows a perspective view of the HO_3 DMBE potential energy surface relevant for the reaction H + O_3 $\rightarrow$ OH + O_2. Because this reaction is highly exothermic and dominated by direct collisions, one may expect such a barrier to play a minor role on the involved dynamics.

Figure 13 shows the corresponding plot for the reaction O + HO_2 $\rightarrow$ OH + O_2. In turn, figure 14 shows a perspective view for the attacking oxygen atom moving in a coplanar manner around the equilibrium HO_2 target molecule. We observe two minima associated with the terminal oxygen atom of the HO_2 radical, and one in the vicinity of its central oxygen atom. The potential energy surface is also seen to be purely attractive when the oxygen atom attacks the molecule along certain nonlinear paths, while the remaining directions offer significant barriers before it can approach the molecule. Such a barrierless optimum reaction path has also been predicted from the MC(DZP) calculations of Dupuis *et al.* [151] but for a perpendicular approach. In fact, simple valence-bond arguments would suggest a sizeable barrier for a coplanar approach of the oxygen atom to HO_2. Yet, it is also true that the full inclusion of

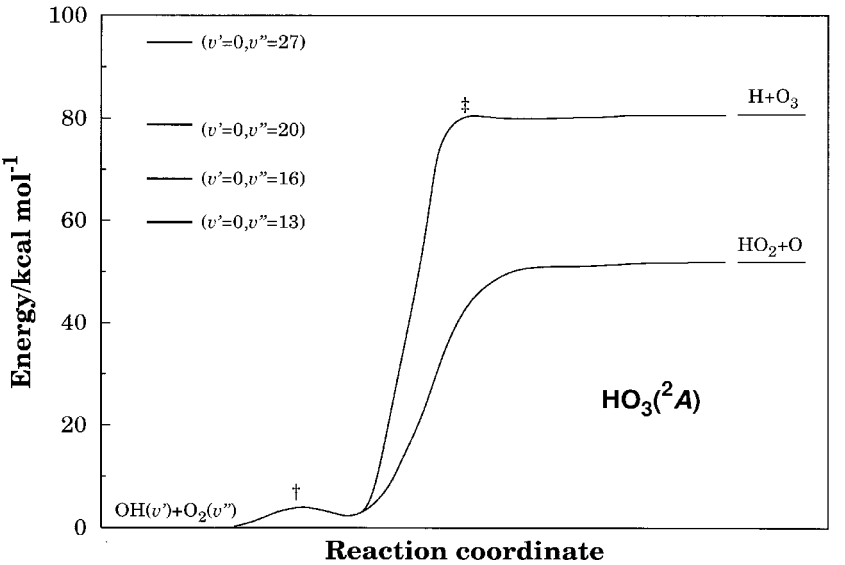

Figure 15. Minimum-energy path for the reactions $OH + O_2 \rightarrow H + O_3$ and $OH + O_2 \rightarrow O + HO_2$. Also indicated are the energies associated with various vibrational combinations of OH $(v') + O_2$ (v'').

electron correlation may alter such a simple analysis. As a result, the disagreement obtained with *ab initio* calculations in predicting a coplanar barrier for both the $H + O_3$ and the $O + HO_2$ channels should not be overemphasized. Figure 14 also shows that the direct abstraction of the hydrogen atom involves a high activation energy and hence is highly unlikely (see section 3.2.3). The energetics are, however, best seen from the plot in figure 15 which shows the minimum-energy path for both the reactions $OH + O_2 \rightarrow H + O_3$ and the reaction $OH + O_2 \rightarrow O + HO_2$. For future reference, we indicate also in this plot the energies associated with various vibrational combinations of OH $(v' = 0) + O_2(v'')$.

3.2.2. *The reaction* $H + O_3 \rightarrow OH + O_2$

The dynamics of the title reaction has been studied on the HO_3 DMBE potential energy surface using both reduced-dimensionality quantum-mechanical IOSA [66, 67] and SP and MP [69] methods, as well as the exact classical approach [125]. The quantum reactive probabilities have been computed by means of equation (35), and the total reactive cross-sections by using equation (54). The calculations have generally been carried out within the j_z approximation using either the five-dimensional polar-averaged potential energy surface $\overline{U}$ of equation (47) or a multiple-path expression of the same function in which the polar angle β is treated as the external parameter. To derive the total wavefunction in the reagents arrangement channel Ψ_{λ_0} (equation (34)), the parameter γ has been treated in the SP and MP [69] methods as a pseudo-IOSA parameter; at each translational distance R, γ was replaced by the SP and MP solution(s) of equation (48) as described in section 2.3.3.

To solve equation (38) for a given ψ_{λ_0}, the translational coordinate R was divided into up to 110 equidistant sectors. In each, one Gaussian (standing as a translational basis function) and a set of twofold adiabatic vibrational basis functions were used (see equation (50)). The number of such functions varied from sector to sector but at each sector their number was constrained using an energy cut-off of 0.5 eV [120, 127]. This

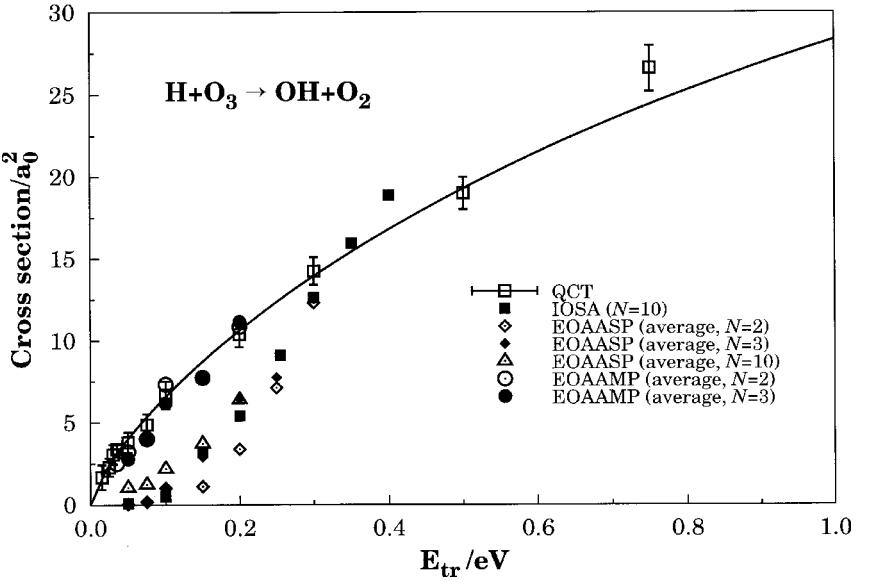

Figure 16. Calculated reactive cross-sections [67, 69, 125] for the reaction $H + O_3 \rightarrow OH + O_2$. N denotes the number of polar angles over which the computed potential U (SP) or cross-sections (MP) have been averaged.

implied solving about 5000 complex equations in order to obtain the coefficients $a^J_{n\lambda}$ in equation (50) [69]. The solution of equation (48) is particularly difficult in the quantum adiabatic methods since the title reaction has more than one reaction track: two due to the two attacking angles, and another two due to the competitive reaction $H + O_3 \rightarrow HO_2 + O$. Once a track is chosen, it is not allowed to mix with another track between different R steps. The track selection was made by using a mask delimiting the range of allowed γ values.

Figure 16 shows the calculated reactive cross-sections for the title reaction. Note that N denotes the number of polar angles over which the computed potential U (SP) or cross-sections (MP) have been averaged. The notable feature from figure 16 is the fact that the average SP and MP quantum results seem to be well converged for $N = 3$. Also interesting is the good agreement between the MP and trajectory results over the range of translational energies where they overlap.

The rate constant has been calculated by means of equation (33), using the appropriate electronic degeneracy factor $g = 1$. Moreover, the calculated cross-sections have been fitted to the form

$$\sigma^r = \frac{C}{E^n} \exp(mE), \tag{56}$$

where C, n and m are least-squares parameters, with equation (56) then being introduced into equation (33) to yield [125, 156]

$$k(T) = C\left(\frac{8k_B T}{\pi\mu}\right)^{1/2} \frac{(k_B T)^n \Gamma(n+2)}{(1 + mk_B T)^{n+2}} \tag{57}$$

The results are shown in figure 17. As expected, the results from the various methods follow the general trend observed above for the cross-section, while showing good agreement with the available experimental measurements [157–162].

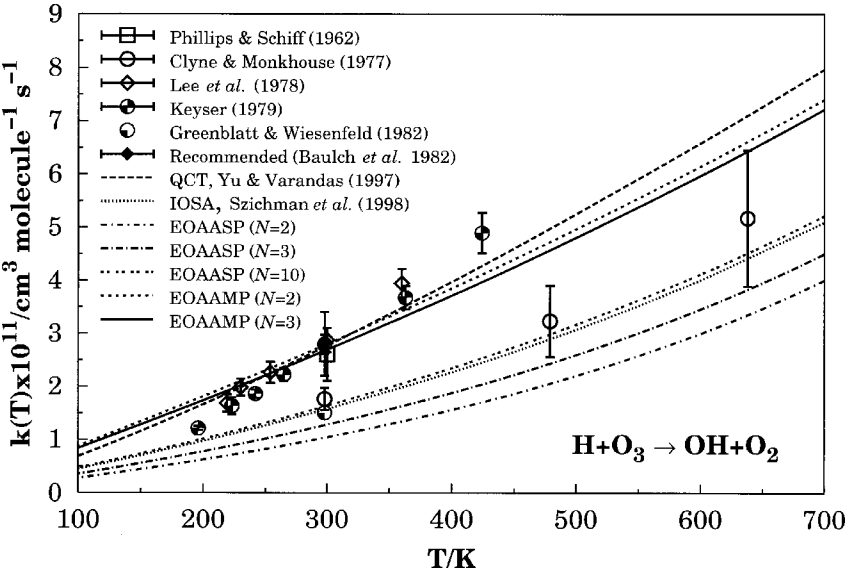

Figure 17. Rate constants for the reaction $H + O_3 \rightarrow OH + O_2$. Besides the theoretical results [66, 69, 125], the results from various experimental groups [157, 159–162] and the recommended values [158] are also shown.

3.2.3. *The reaction* $O + HO_2 \rightarrow OH + O_2$

The title reaction was also studied on the HO_3 DMBE potential energy surface, employing both reduced-dimensionality IOSA and SP quantum methods [68] as well as the trajectory approach [163]. In this section, we survey briefly these calculations.

First, we note that two possible mechanisms can be offered to explain the title reaction

$$O_a + HO_b\,O_c \rightarrow O_a\,H + O_b\,O_c, \tag{58}$$

$$O_a + HO_b\,O_c \rightarrow O_b\,H + O_a\,O_c, \tag{59}$$

where the subscripts a, b and c label the three different oxygen atoms. Clearly, equation (58) corresponds to a hydrogen-atom abstraction mechanism while equation (59) refers to an oxygen-atom abstraction mechanism. Although both mechanisms have been advanced [164], the kinetic measurements [165–167] suggest that the title reaction should occur preferentially via the oxygen-atom abstraction. Such an oxygen-atom abstraction mechanism has in fact been confirmed experimentally [168] via ^{16}O–^{18}O substitution and supported theoretically through the trajectory calculations [163]. Indeed, out of 8000 calculated trajectories, none leads to the reaction (58).

In the quantum approaches, the reactive probabilities have been computed by means of equation (35), and wholly attributed to the reaction leading to $OH + O_2$ as suggested from the trajectory calculations [163] for the considered high-energy conditions. The calculations were generally carried out within the j_z approximation using a polar-averaged expression of the potential energy surface. As usual, in IOSA, the perturbed part of the total wavefunction in the reagents arrangement χ_{λ_0} has been obtained by treating γ as a parameter. In agreement with [163], the reactive region was found to cover γ values between 0 and 80°.

To solve equation (38), the R-translational axis has been divided into up to 180 equidistant sectors. Each of these included one Gaussian, standing as a translational basis function, and a set of twofold adiabatic vibrational basis functions (see equation

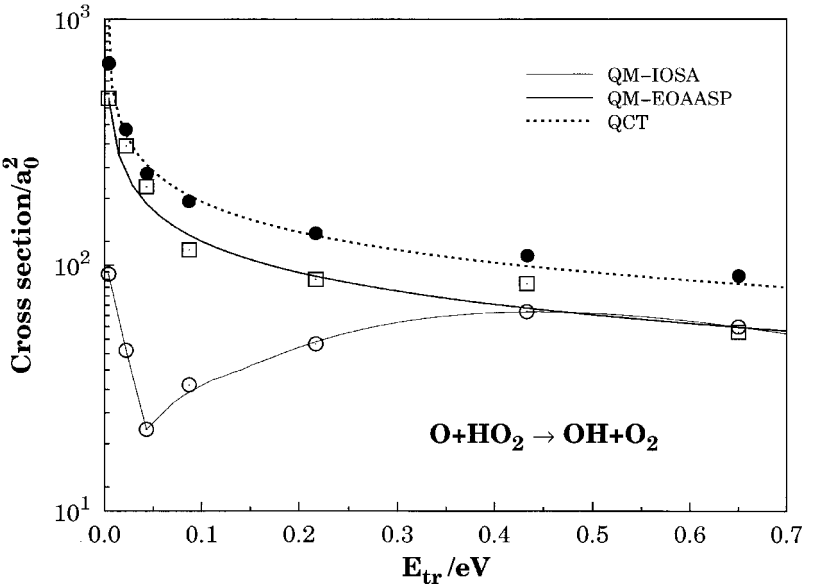

Figure 18. Classical [125] quantum-mechanical (QM) IOSA [68] and quantum-mechanical (QM) SP [68] cross-sections for the reaction $O + HO_2 \rightarrow OH + O_2$ as a function of the translational energy.

(50)). Since the OH bond behaves essentially like a spectator [163], a single vibrational basis function along this axis was judged sufficient to accurately describe its relaxation. Conversely, as expected from the results of [163] (where highly excited O_2 product molecules have been shown to be formed), at least 50–60 basis functions needed to be considered along the ρ coordinate to describe correctly these twofold adiabatic vibrational basis functions. Their total number per sector was then constrained by using a cut-off energy value of 1.8 eV [120, 127], which implied the solution of about 4000 complex equations in order to obtain the coefficients $a^J_{n\lambda}$ in equation (50).

As in section 3.2.2, it was particularly difficult to implement the calculations using the average potential described in equation (47) owing to the large anisotropy in β of the HO_3 DMBE potential energy surface. For simplicity, the potential was averaged using only two angles ($\beta = 0$ and 180°), that is only coplanar configurations have been considered. Note that, even if further β values were taken into consideration for the averaging procedure, the real six-dimensional problem would still be converted into a pseudo-coplanar problem. Note further that the exact treatment of a coplanar reaction would require a five-dimensional treatment, and hence the three-dimensional study represents a reduced-dimensionality analysis even for a coplanar situation. Although such averaging approximation is not expected to affect the essentials of the calculations drastically, and has indeed been frequently used by other workers [114, 169, 170] further investigation would be valuable.

Figure 18 compares the calculated cross-sections (classical, and quantum IOSA and SP) for the $O + HO_2$ reaction as a function of the translational energy. The calculated IOSA cross-sections show, on decreasing the collisional energy, a rapid decline at first and then a sharp increase at very low energies. Such a trend contrasts with the classical and SP results. This has been attributed to the averaging procedure in equation (53), and the fact that only the sampled angles close to the optimum path lead to reaction. The fact that the trajectory results at high energies are still larger than

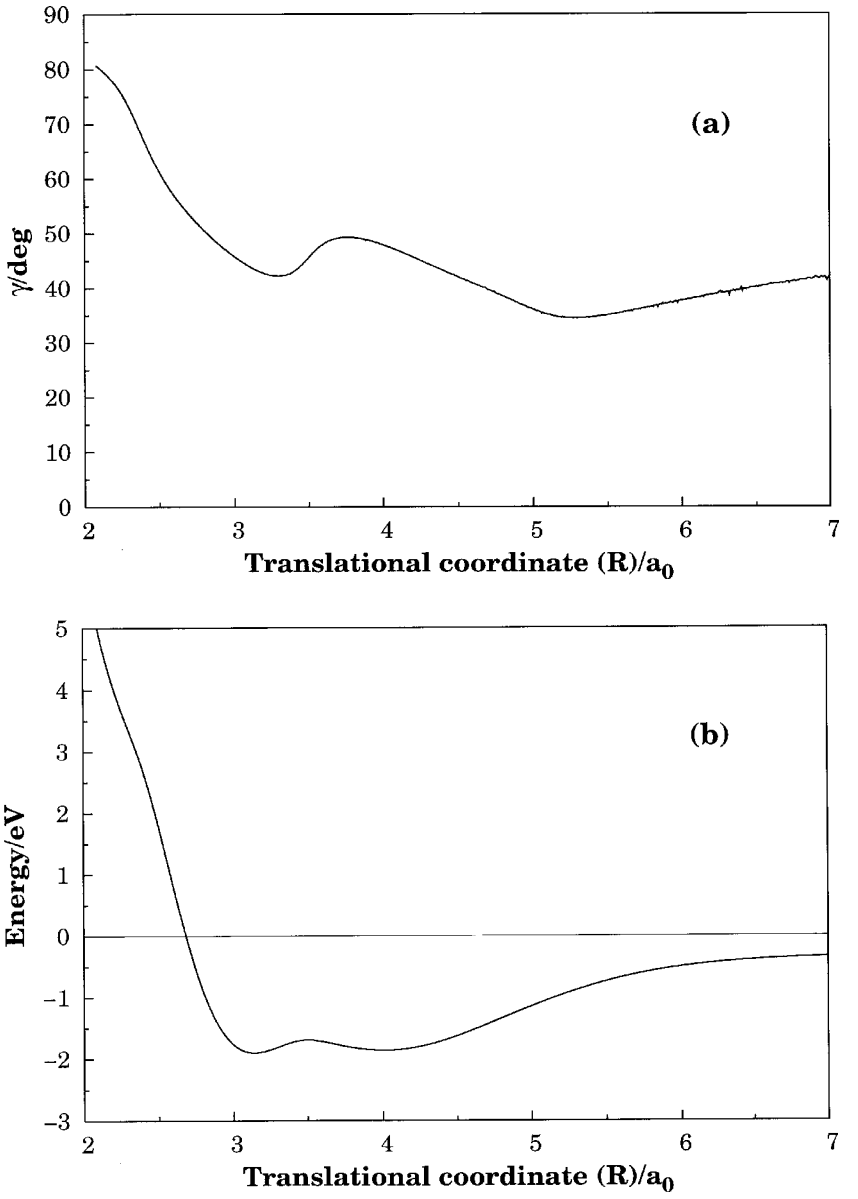

Figure 19. Calculated values of (*a*) the optimum angle and (*b*) the energy along the reaction path shown as functions of the translational distance *R*.

IOSA was explained as due to the narrow cone of acceptance for the title reaction. In fact, the classical method appears to direct more trajectories to the reaction region which may be explained as due to a reorientation of the HO_2 molecules as the oxygen atom approaches it so as to find the optimum reaction pathway. This looks a fair explanation, since the incoming oxygen atom tends to attack the terminal oxygen atom of the triatomic molecule and the hydrogen atom is light (thus, the HO_2 molecule can easily rotate to offer the terminal oxygen atom to the homologous attacking atom).

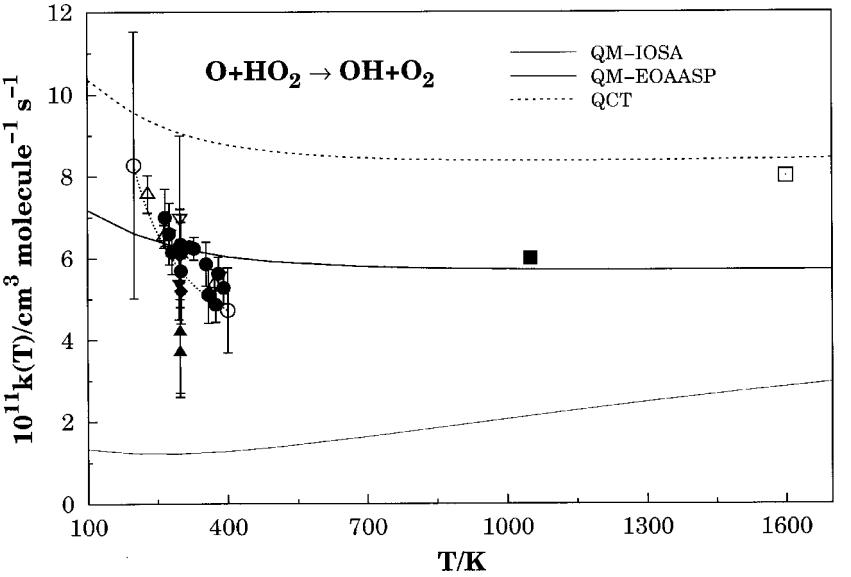

Figure 20. Thermal rate coefficients as a function of temperature for the reaction $O + HO_2 \rightarrow OH + O_2$. The lines indicate the calculated values (QM, quantum mechanical) [68, 162] while the experimental results [165–167, 173–178] are indicated by the symbols.

Figure 18 also shows that, at high energies, both IOSA and SP quantum-mechanical approaches give the same results, although they rely on opposite principles. This is because at high energies the path followed during the collisional process is irrelevant. Clearly, the SP method gives better agreement with the trajectory predictions at lower energies and follows the typical capture-type behaviour. Tentatively, the fact that the trajectory calculations exceed the SP data was partly attributed to zero-point energy leakage [16–33].

In turn, figure 19 shows the calculated SP values of the optimum angle and energy along the reaction path as a function of the translational coordinate R. Their behaviour looks smooth and acceptable, showing no barriers to the incoming oxygen atom. Note that the quantum-mechanical adiabatic path approach implies replacing the value of γ in equations (35)–(52) by the value of γ_{SP} as defined in equation (48). Thus, the application of equation (53) becomes unnecessary since the calculations are carried out only once on a single optimum γ path.

The calculated thermal rate coefficients are shown in figure 20 as a function of temperature for 100 K $\leqslant T \leqslant$ 1700 K. The following electronic degeneracy factor has been employed

$$g(T) = \frac{1}{5 + 3\exp(-227.6/T) + \exp(-325.9/T)}, \tag{60}$$

which accounts for the electronic degeneracies of $O(^3P) + HO_2(^2A'')$ and the fact that the DMBE potential energy surface refers to $HO_3(^2A)$ [50, 163, 171, 172]. In turn, the IOSA cross-sections have been described by the form

$$\sigma_{IOSA}^{\Gamma} = \frac{C_1}{E^{n_1}} + C_2 E^{n_2} \exp(-m_1 E), \tag{61}$$

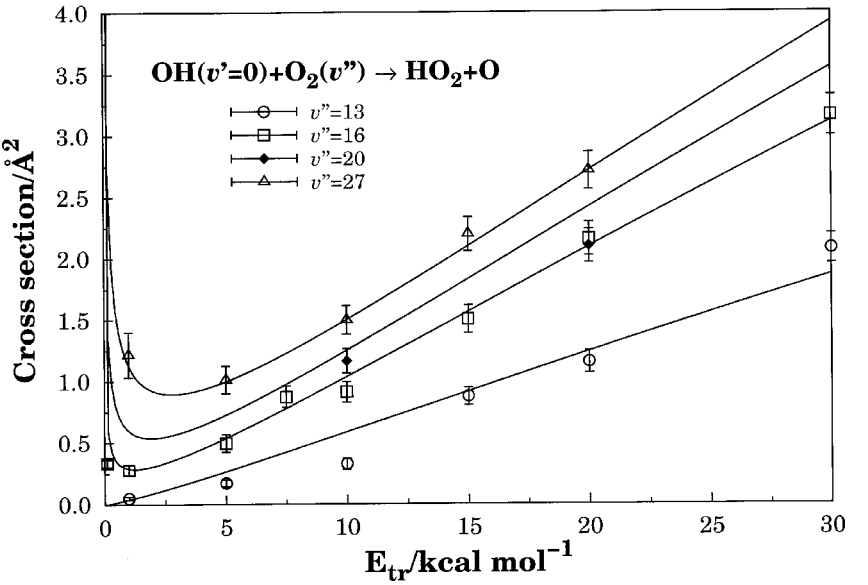

Figure 21. Excitation functions [179] for the OH ($v' = 0$) + O_2 (v'') reaction with the molecules in their ground rotational states ($j_{OH} = j_{O_2} = 1$). Also shown are the associated 68% error bars, and the best-line fits using equation (63).

while the SP cross-sections were best fitted using

$$\sigma_{SP}^{r} = \frac{C_3}{E^{n_3}} \exp(-m_2 E), \tag{62}$$

where C_i, n_i and m_i are adjustable parameters. Also included for comparison are the results from available experimental measurements [165–167, 173–178] and those from the trajectory calculations [163]. Clearly, there is good agreement between the theoretical methods, and between these and the experimental results.

3.2.4. *The reactions* $OH(v') + O_2(v'') \rightarrow O + HO_2$ *and* $OH\ (v') + O_2\ (v'') \rightarrow H + O_3$

Calculations were also recently reported [179] for the title reactions using the QCT method and the HO_3 DMBE potential energy surface. The calculated cross-section versus translational energy curves for the colliding molecules in their ground rotational states ($j_{OH} = j_{O_2} = 1$) are given in figure 21 together with the associated 68% error bars. Two opposite trends may explain their shape. At low energies, the capture-type regime dominates leading to the well established (for example [3, 163, 180], and references therein) decreasing dependence of σ^r with E_{tr}. At high energies, the observed pattern is more typical of a reaction having an energy threshold (i.e. σ^r is an increasing function of E_{tr}). As a result, the excitation function shows a minimum in the region where the two effects balance each other. Figure 21 gives also for comparison the best fits based on the function

$$\sigma_{0v''}^{r} = C\frac{v'' - v_{th}}{E_{tr}^{n}} + B_{v''} E_{tr}^{6/5} \exp(-mE_{tr}), \tag{63}$$

where v_{th} is the threshold vibrational quantum number, $m = 0.008$ mol kcal^{-1} is a decay factor (assumed to be constant for all cases), and the coefficient $B_{v''}$ is a function

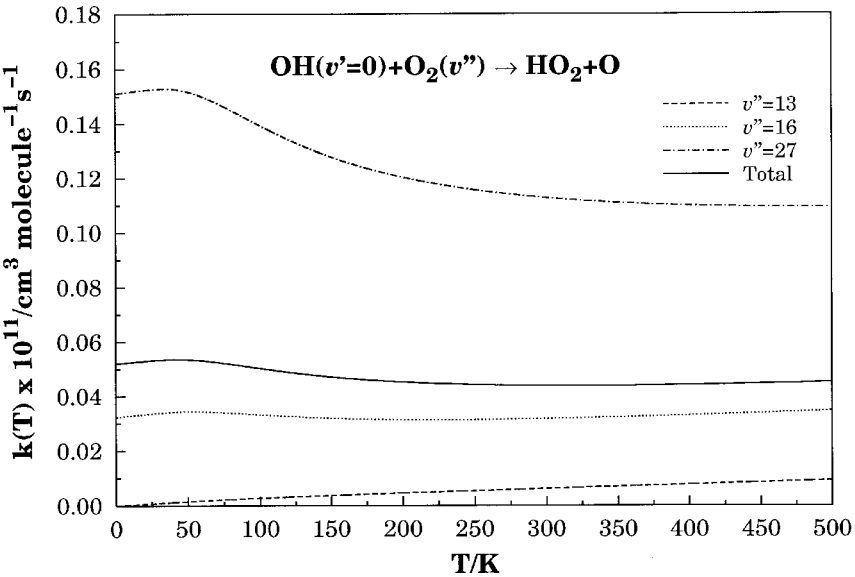

Figure 22. Equation (65) for vibrational quantum numbers of O_2 equal to $v'' = 13$, 16, and 27 [179]. Also indicated is the vibrationally averaged thermal rate coefficient given by equation (67). For the weights, see the text.

of the vibrational quantum number. Note that the power of E_{tr} in the capture-type term is $m = \frac{1}{2}$, which is the value expected for a dipole–quadrupole electrostatic interaction (i.e. $n = \frac{2}{4}$). In turn, $B_{v''}$ was assumed to be a Taylor series expansion around $v'' = 13$ truncated at fifth order, namely

$$B_{v''} = \sum_{k=0}^{4} b_k (v'' - 13)^k, \tag{64}$$

while C and b_k are least-squares parameters. Also shown in figure 21 is the curve for $v'' = 20$; the two calculated points (not fitted) for this vibrational combination show that equation (63) provides a reliable fit over most values of v''. Substitution of equation (63) into equation (33) leads to the following specific thermal rate coefficient:

$$k_{0v''}(T) = f(T)\left(\frac{2}{k_B T}\right)^{3/2}\left(\frac{1}{\pi\mu}\right)^{1/2}\left(C_{v''}(k_B T)^{3/2}\Gamma(\tfrac{3}{2}) + B_{v''}\frac{\Gamma(\frac{16}{5})}{(0.008 + 1/k_B T)^{16/5}}\right) \tag{65}$$

where $C_{v''} = C(v'' - 13)$, $\Gamma(\cdot)$ is the gamma function, and

$$f(T) = \frac{1}{3}\frac{1}{1 + \exp(-205/T)} \tag{66}$$

is the factor which accounts for the electronic degeneracies in the title reaction.

Figure 22 shows $k_{0v''}(T)$ for values of v'' equal to 13, 16 and 27. Also indicated is the vibrationally averaged thermal rate coefficient given by

$$k(T) = \frac{\Sigma_{v''}\,\omega_{v''}k_{0v''}(T)}{\Sigma_{v''}\,\omega_{v''}}, \tag{67}$$

where the populations $\omega_{v''}$ for the vibrational state v'' have been assumed to be those obtained in the 226 nm photolysis of ozone [9]. Note that the limits of $k(T)$ are

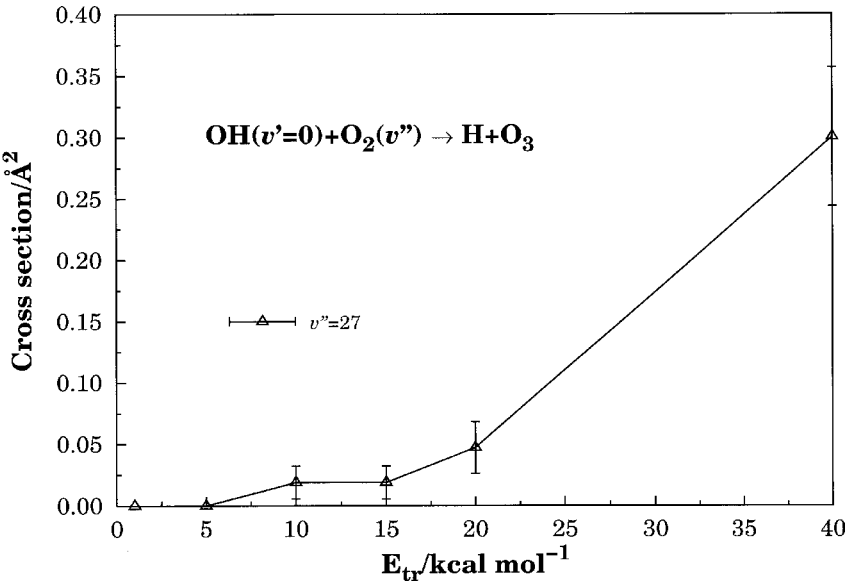

Figure 23. Excitation function [179] for the reactive channel leading to ozone formation. The calculations were made for $j_{HO} = 10$ and $j_{O_2} = 9$.

essentially determined by the electronic degeneracy factor $f(T)$. In particular it determines the increase in the specific rate constant for very small temperatures, a feature which may have importance in atmospheric chemistry at high altitudes. No attempt was made to correct for zero-point energy leakage [16–33]. Although all reactive trajectories were found to lead to HO_2 molecules with a total vibrational energy which exceeds its overall zero-point energy value, it was not possible to check whether that was true for each normal mode. Moreover, 20–30% of the non-reactive trajectories yielded OH with an energy below its zero-point value. Because of this, it was believed that the calculated reactive cross-sections underestimated their true values. In turn, preliminary calculations for $j_{OH} = 10$ and $j_{O_2} = 9$ have shown that the inclusion of rotational excitation in OH has a significant effect on the reactive probability only at low energies. This is believed to be primarily due to an increase in the available energy content and orientational effects, with the latter being expected to be more relevant at low energies since the molecules have then time to reorient and find the optimum orientation for reaction.

Other reactive channels have also been investigated [179] for the case when the vibrational quantum number of the oxygen molecule is $v'' = 27$. All such channels have shown a small reactive cross-section. Of particular interest is that forming ozone, which was found to become relevant only at high translational energies, as shown in figure 23. In this case, the calculations made for $j_{HO} = 10$ and $j_{O_2} = 9$ have indicated that the addition of rotational energy in the reactants also enhances ozone formation, especially in the high-translational-energy regime. This is most probably an energy effect, since orientational effects are expected to be less important in this high-energy regime (i.e. the molecules do not have time to find the optimum orientation for reaction). Finally, no breaking of the OH bond was observed, with HO_2 formation occurring via a capture-type (barrier-type) mechanism for low (high) translational energies. Although no comparison with experimental data has been possible, the calculations suggest that laser experiments which allow the preparation of vibration-

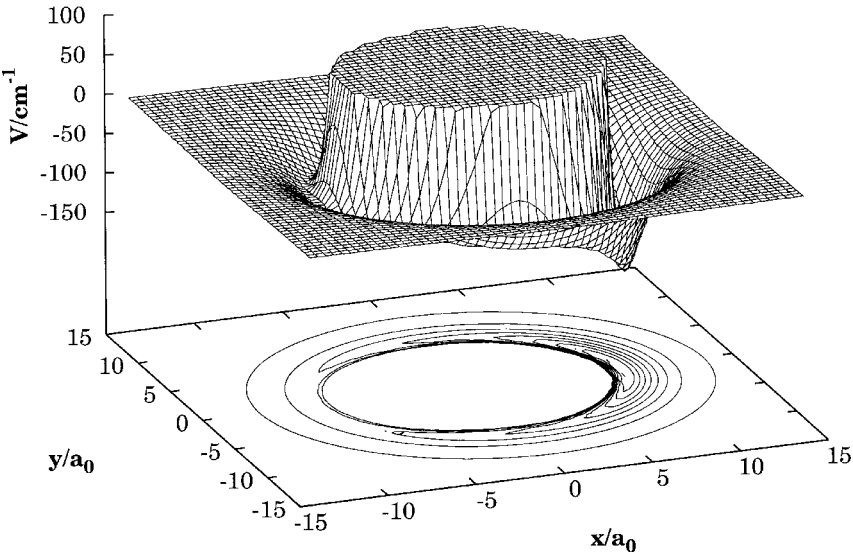

Figure 24. Perspective view and contour plot of the DMBE potential energy surface for argon moving around an equilibrium HCN [181] molecule.

ally hot reactant molecules may be used to control the outcoming products of the OH $(v') + O_2$ (v'') reaction.

3.3. *The Ar + HCN dissociation reaction and its reverse*

3.3.1. *The ArHCN potential energy surface*

The ArHCN potential energy surface has been written as [48]

$$V_1(\mathbf{R}) = \sum_{\beta=C,N,H} V^{(2)}_{A r_\beta}(R_{A r_\alpha}) + V^{(3)}_{HCN}(R_{CN}, R_{CH}, R_{NH}), \tag{68}$$

where $\mathbf{R}$ is the collective variable of the six internuclear distances. Thus, it is of DMBE type, with the pair-potentials assuming the extended Hartree–Fock approximate correlation energy (EHFACE2) form [37]; the short-range Hartree–Fock energy is represented by a Born–Mayer curve, and the dynamical correlation is modelled semiempirically from the atom–atom damped dispersion series expansion.

More recently [76], an improved HCN surface has been reported from the ES scheme [77, 78]. Thus, it has the form (17), with $V_1(\mathbf{R})$ being the DMBE potential energy surface [181] referred to in the previous paragraph, and $V_2(\mathbf{R}')$ the *ab initio* potential of Clary *et al.* [182] for the Ar…HCN van der Waals interaction. This assumed the form [181]

$$V_2(\mathbf{R}) = V_{HCN}(R_{CN}, R_{CH}, R_{NH}) + \sum_{n=0}^{6} c_n(R)\, P_n(\cos\theta), \tag{69}$$

where the second term is an *ab initio* atom-rigid triatom potential function similar to that of [182]. Thus, R is the vector that joins the argon atom to the centre of mass of the HCN molecule, and θ is the angle of orientation of this vector with respect to that (r) defined by the HCN axis. In turn, $P_n(\cos\theta)$ is a Legendre polynomial, and

$$c_n(R) = \left(\sum_{k=0}^{3} \tilde{A}_{nk}\, R^k \exp(-2R) \right) + \chi_6(R) \frac{\tilde{A}_{n4}}{R^6}, \tag{70}$$

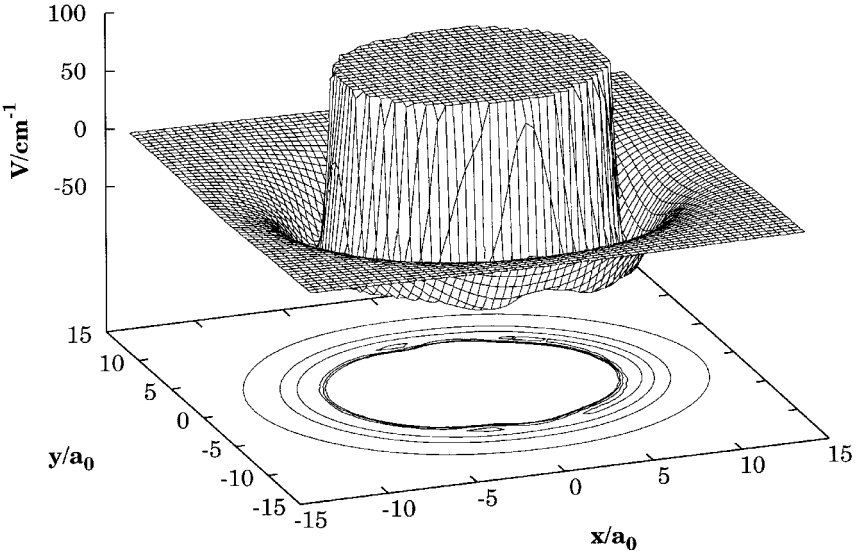

Figure 25. As in figure 24 but for the ES potential energy surface of ArHCN [76].

with $\chi_6(R)$ being a dispersion damping function similar to that employed for atom–atom interactions [37, 81, 183]. Note that $V_{\rm HCN}$ in equation (69) is the DMBE potential energy surface [48] for HCN, which introduces the proper dependence on the intramolecular degrees of freedom. Thus, $\mathbf{R}'$ in equation (69) is a collective variable of only five coordinates since the van der Waals potential form assumes a rigid triatomic HCN molecule. In spite of this, the results showed that the ES approach warrants a smooth transition from the low-energy regions, where the van der Waals potential $V_2(\mathbf{R}')$ is valid, to the high-energy regions where $V_1(\mathbf{R}')$ is expected to dominate and provide an acceptable representation of the true ArHCN potential energy surface. We further observe that the radial part of the van der Waals potential has the standard form of a polynomial multiplied by an exponential for the short-range term and a damped attractive R^{-6} term for the long range part. This differs from the form used by Clary *et al.* [182] only in the dispersion damping functions. These assumed [48] a form similar to that employed for the induced dipole-induced dipole atom–atom dispersion damping function [37, 81, 183] and hence has been constructed under the assumption that HCN may be replaced by the corresponding isoelectronic atom (i.e. Si). Thus, although this may be questionable, its θ dependence has been ignored. Moreover, the leading coefficients of the induction and dispersion series expansions, which characterize the Ar$\cdots$HCN van der Waals interaction and are known to vary as R^{-6}, have been treated jointly.

Figure 24 shows the DMBE potential energy surface for ArHCN while the ES potential energy surface is in figure 25. Note that this surface corresponds to ES III in [76], a notation which we keep here for consistency. It should be observed that the *ab initio* potential V_2 used to construct ES III has been slightly tuned to adjust the vibrational–rotational data on the ArHCN van der Waals molecule, which is known from spectroscopic measurements [184, 185]. Although similar, there are topographic differences between the two potential energy surfaces which justify their distinct vibrational–rotational spectra [76], as shown in figure 26. Note that, besides the calculated vibrational levels of even (e) and odd (f) parity, figure 26 illustrates the

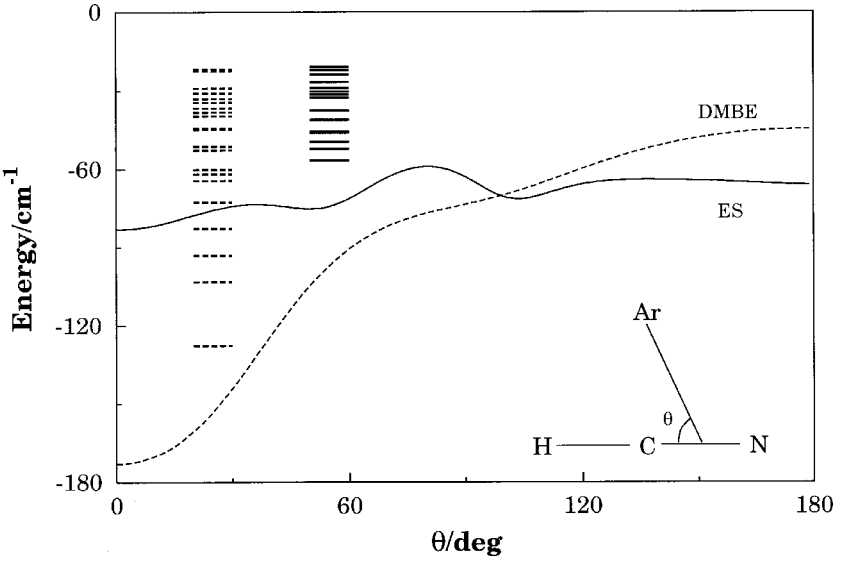

Figure 26. A comparison of the DMBE and ES potential energy surfaces for the minimum-energy path corresponding to argon moving around an equilibrium HCN molecule. Also shown by the bars on the left-hand side is a comparison of the calculated vibrational levels for the two surfaces.

minimum-energy path for argon moving around HCN which has been fixed at its linear equilibrium geometry. Clearly, the ES III potential shows a kind of T-shaped van der Waals minimum which is absent in the DMBE potential energy surface (see figure 24). In turn, the minimum shown by the latter for collinear geometries is considerably deeper than that of ES III. However, as expected, such small though significant differences in the vibrational spectra have no implication on the dynamics of the title reaction which we discuss next.

3.3.2. *The reaction Ar + HCN → Ar + H + CN*

The title reaction has been studied for a wide range of initial vibrational and translational energies using classical dynamics and the realistic DMBE potential energy surface for ArHCN. This reaction and its reverse recombination process are an important class of elementary reactions which are involved in combustion chemistry. Indeed, according to the Lindemann approach and its subsequent refinements, namely the extensively tested and widely accepted [186] Rice–Ramsperger–Kassel–Marcus (RRKM) scheme, unimolecular reactions become pressure dependent in the so-called low-pressure limit which is attained when the collisional excitation and de-excitation processes are dominant. At the high temperatures reached in flames, these processes govern the kinetics and the low-pressure limit rate constants become very important to rationalize such reactions. Of course, if Ar is assumed to be representative of a closed-shell third body, then the Ar + HCN reaction can be a relevant model for propellant combustion reactions, and more generally for combustion of nitrogen-containing materials at high temperatures [13]. Although these reactions were not considered by Miller and Bowman [14] on the combustion of nitrogen compounds (they considered temperatures up to 2500 K), the HCN removal by dissociation is expected for high temperatures to be competitive with oxidation by atomic oxygen.

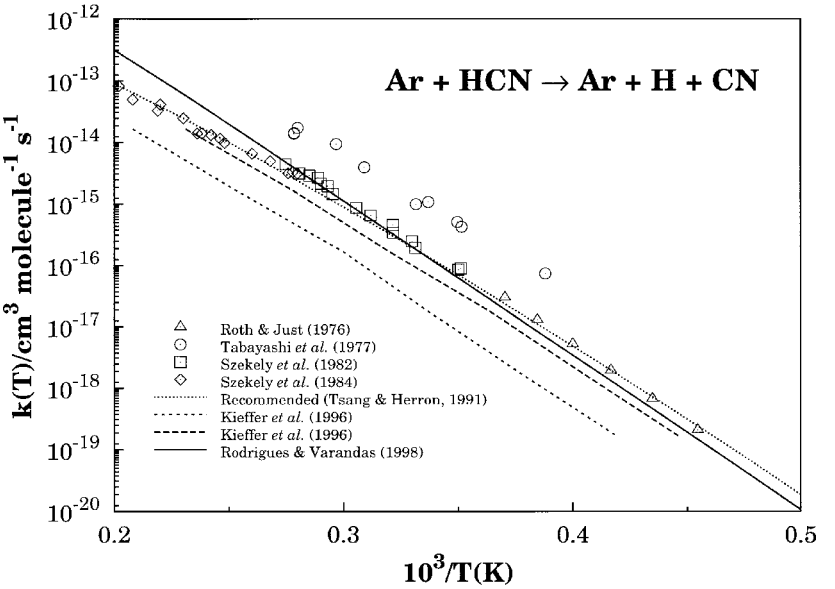

Figure 27. Dependence on temperature of the calculated thermal rate coefficient [181] for the reaction Ar + HCN → Ar + H + CN. Also shown are previous recommended [13], experimental [188–191] and theoretical [192], results.

For the dynamics, the following fundamental assumptions have been made.

(*a*) The reaction occurs only on the ground potential energy surface of ArHCN.
(*b*) The model potential energy surface describes accurately the reactive paths.
(*c*) The classical trajectory method is adequate for studying the title reaction.
(*d*) Below the classical dissociation limit the HCN molecules are in thermal equilibrium.
(*e*) The density of states, $\rho(E)$, can be described by a classical continuous function which can be approximated using the harmonic approximation.

Such assumptions have been found to be acceptable, with (*d*) and (*e*) being the most problematic. An extra assumption concerned the definition of the HCN internal energy.

(*f*) The internal energy of HCN was taken to be only vibrational.

Thus, the angular momentum component perpendicular to the molecular axis was assumed to be vanishingly small, which implies beginning the trajectories with no rotational energy. Because HCN is a linear molecule, a vibrational angular momentum l will appear [187]. This was taken into account by making a microcanonical sampling of the internal energy, which has been distributed through the four normal modes of vibration: the degenerate bending modes and the two stretching modes.

The dependence on temperature of the calculated thermal rate coefficient is illustrated in figure 27. Also shown for comparison are known experimental [188–191] and recommended [13] values. The theoretical RRKM-type calculations of Kiefer *et al.* [192] are also indicated. Clearly, the agreement with experiment is good except at high temperatures. This was attributed [181] to the use of rotationally cold molecules and the fact that the expected non-thermal distribution near dissociation was not

taken into account. Of course, the contribution of excited electronic states cannot also be totally disregarded in such high-temperature regimes.

4. Concluding remarks

In this review we have discussed the energetics and dynamics of seven reactions using either quantum-mechanical or classical methods. In some cases both these approaches have been employed and the results were compared with each other. In all cases the potential energy surfaces have been based on *ab initio* electronic structure calculations, although some fine tuning was then used to model the final global functions. This was achieved by using the DMBE approach alone or in combination with the ES method. The quantum dynamics studies were carried out in a consistent way within the IOSA approximation or the novel elastic adiabatic optimum angle approaches. All studies were based on the premise that non-adiabatic effects could be ignored.

Six of the reactions studied in the present review have great relevance in stratospheric ozone chemistry. Although they are only a subset of the reactions necessary for modelling the chemistry of stratospheric ozone, such reactions are the most influential since only natural species are involved which have a high abundance in the atmosphere. Thus, they may be used to provide a model prediction from first principles of an oxygen–hydrogen atmosphere in which contamination by other chemicals is absent. Also reviewed was a reaction involving collisional-induced dissociation of HCN, which is more relevant in modelling the combustion of nitrogen-containing materials. In all cases, general good agreement was achieved with the available experimental kinetics data. Yet, some significant differences exist between the transition state attributes of the model DMBE potential energy surfaces and those obtained from recent *ab initio* studies. Work to clarify these issues, including new *ab initio* calculations, are currently under way in our group. Finally, there are no reasons of principle why the methods discussed in this account cannot be successfully generalized to other four-atom and larger polyatomic reactions which are currently at the forefront of reaction dynamics. Indeed, work is in progress in our group to study the five-atom $HO + O_3$ and $O_2 + O_3$ reactions, which is also of great relevance in the depletion cycle of stratospheric ozone. Similarly, exploratory work is being carried out to study collisional processes involving as many as six ($HO_2 + O_3$, and $O_3 + O_3$) ground-state atoms.

Acknowledgements

I thank all my coworkers for their valuable contributions. This work has the support of the Fundação para a Ciência e Tecnologia, Portugal, under programme PRAXIS XXI.

Note added in proof: While this work was in proof stage, trajectory calculations for the $OH(v',j') + O_2(v'',j'')$ reaction were completed [193] covering many vibrational–rotational combinations of the reactant molecules. The results have confirmed that ozone formation can be enhanced greatly by vibrationally exciting the OH reactant molecule. Equation (63) has also been generalized to cover the vibrational–rotational preparation of both reactant species by obtaining an expression which encompasses the various combinations of the reactants' internal energies. As a result, a general expression for the state resolved rate constants in equation (65) was also determined. Finally, a preliminary study of the $OH + O_3$ reaction has been carried out [194] using a HO_4 DMBE potential energy surface constructed from the available many-body

energy terms up to four-body. The results are promising and suggest that a simple five-body energy term may suffice to fine tune the current HO_4 DMBE surface such as to produce rate constants in good agreement with the available experimental results.

Appendix A. Proof of equation (36)

Consider the one-dimensional Schrödinger equations for the perturbed and unperturbed (elastic) systems, namely

$$-\frac{\hbar}{2\mu}\Psi'' + (W - E)\,\Psi = 0, \tag{A 1}$$

$$-\frac{\hbar}{2\mu}\psi'' + (W_0 - E)\,\psi = 0, \tag{A 2}$$

where the double prime stands for second derivative with respect to the spatial coordinate x, and

$$\Psi = \chi + \psi, \tag{A 3}$$

$$W = W_0 + V, \tag{A 4}$$

with ψ and W_0 being the wavefunction and potential respectively of the unperturbed system. By replacing equations (A 3) and (A 4) in equation (A 1), one then obtains

$$\frac{\hbar}{2\mu}\chi'' + (E - W)\,\chi = V\psi, \tag{A 5}$$

which proves equation (38) in the text.

Multiplying now equation (A 5) on the left by ψ^*, and the conjugate of equation (A 2) on the right by χ, one obtains after subtracting them and integrating by parts

$$\frac{\hbar}{2\mu}(\psi'^*\chi' - \psi^*\chi') + \langle \psi |\, V \,|(\chi + \psi)\rangle = 0. \tag{A 6}$$

Finally, by writing the wavefunctions as

$$\lim_{x\to\infty} \Psi = \left(\frac{1}{k}\right)^{1/2} [\exp(-\mathrm{i}kx) + S\exp(\mathrm{i}kx)] \tag{A 7}$$

$$\lim_{x\to\infty} \psi = \left(\frac{1}{k}\right)^{1/2} [\exp(-\mathrm{i}kx) + \exp(\mathrm{i}kx + \phi)] \tag{A 8}$$

where $k = (2\mu E_{\mathrm{tr}}/\hbar)^{1/2}$, one obtains after some algebraic manipulation

$$S = \left(1 + \frac{\mu}{\mathrm{i}\hbar}\langle \psi |\, V \,|(\chi + \psi)\rangle\right)\exp(\mathrm{i}\phi). \tag{A 9}$$

Since this includes only elastic scattering, it may then be generalized to the desired result by writing

$$S = \left(\delta_{\lambda\lambda_0} + \frac{\mu}{\mathrm{i}\hbar}\langle \psi_\lambda |\, V \,|(\chi_{\lambda_0} + \psi_{\lambda_0})\rangle\right)\exp(\mathrm{i}\phi_\lambda), \tag{A 10}$$

where $\delta_{\lambda\lambda_0}$ is the Kronecker delta function, and λ (λ_0) stands for a full set of quantum numbers which label the state of the interacting particles.

References

[1] NICOLET, M., 1984, *Adv. chem. Phys.*, **55**, 63.
[2] VARANDAS, A. J. C., PAIS, A. A. C. C., MARQUES, J. M. C., and WANG, W., 1996, *Chem. Phys. Lett.*, **249**, 264.
[3] MARQUES, J. M. C., WANG, W., PAIS, A. A. C. C., and VARANDAS, A. J. C., 1996, *J. phys. Chem.*, **100**, 17513.
[4] FROIDEVAUX, L., ALLEN, M., and YUNG, L. Y., 1985, *J. geophys. Res.*, **90**, 12999.
[5] CLANCY, R. T., RUSCH, D. W., THOMAS, R. J., ALLEN, M., and ECKMAN, R. S., 1987, *J. geophys. Res.*, **92**, 3067.
[6] SLANGER, T. G., 1994, *Science*, **265**, 1817.
[7] SLANGER, T. G., JUSINSKI, L. E., BLACK, G., and GADD, G. E., 1988, *Science*, **241**, 945.
[8] PARKER, H., and SLANGER, T. G., 1994, *J. chem. Phys.*, **100**, 287.
[9] MILLER, R. L., SUITS, A. G., HOUSTON, P. L., TOUMI, R., MACK, J. A., and WODTKE, A. M., 1994, *Science*, **265**, 1831.
[10] PRICE, J. M., MACK, J. A., ROGASKI, C. A., and WODTKE, A. M., 1993, *Chem. Phys.*, **175**, 83.
[11] ROGASKI, C. A., PRICE, J. M., MACK, J. A., and WODTKE, A. M., 1993, *Geophys. Res. Lett.*, **20**, 2885.
[12] DRABBLES, M., and WODTKE, A. M., 1999, *J. phys. Chem.* A, **103**, 7142.
[13] TSANG, W., and HERRON, T., 1991, *J. phys. Chem. Ref. Data*, **20**, 609.
[14] MILLER, J. A., and BOWMAN, C. G., 1989, *Prog. Energy Combust. Sci.*, **15**, 287.
[15] RODRIGUES, S. P. J., and VARANDAS, A. J. C., 1999, *J. phys. Chem.*, **103**, 6366.
[16] BOWMAN, J. M., GAZDY, B., and SUN, Q., 1989, *J. chem. Phys.*, **91**, 2859.
[17] MILLER, W. H., HASE, W. L., and DARLING, C. L., 1989, *J. chem. Phys.*, **91**, 2863.
[18] NYMAN, G., and DAVIDSSON, J., 1990, *J. chem. Phys.*, **92**, 2415.
[19] ALIMI, R., GARCÍA-VELA, A., and GERBER, R. B., 1992, *J. chem. Phys.*, **96**, 2034.
[20] VARANDAS, A. J. C., and MARQUES, J. M. C., 1992, *J. chem. Phys.*, **97**, 4050.
[21] VARANDAS, A. J. C., 1993, *J. chem. Phys.*, **99**, 1076.
[22] PESLHERBE, G. H., and HASE, W. L., 1994, *J. chem. Phys.*, **100**, 1179.
[23] VARANDAS, A. J. C., and MARQUES, J. M. C., 1994, *J. chem. Phys.*, **100**, 1908.
[24] VARANDAS, A. J. C., 1994, *Chem. Phys. Lett.*, **225**, 18.
[25] BEN-NUM, M., and LEVINE, R. D., 1994, *J. chem. Phys.*, **101**, 8768.
[26] LIM, K. F., and MCCORMACK, D. A., 1995, *J. chem. Phys.*, **102**, 1705.
[27] KUMAR, S., SATHYAMURTHY, N., and RAMASWAMY, R., 1995, *J. chem. Phys.*, **103**, 6021.
[28] SCHLIER, C., 1995, *J. chem. Phys.*, **103**, 1989.
[29] MCCORMACK, D. A., and LIM, K. F., 1995, *J. chem. Phys.*, **103**, 1991.
[30] GUO, Y., THOMPSON, D. L., and SEWELL, T. D., 1996, *J. chem. Phys.*, **104**, 576.
[31] BEN-NUN, M., and LEVINE, R. D., 1996, *J. chem. Phys.*, **105**, 8136.
[32] MCCORMACK, D. A., and LIM, K. F., 1997, *J. chem. Phys.*, **106**, 572.
[33] LIM, K. F., 1997, *J. chem. Soc., Faraday Trans.*, **93**, 669.
[34] VARANDAS, A. J. C., and MIL'NIKOV, G. V., 1996, *Chem. Phys. Lett.*, **259**, 605.
[35] MIL'NIKOV, G. V., and VARANDAS, A. J. C., 1999, *Phys. Chem. chem. Phys.* **1**, 1071.
[36] MIL'NIKOV, G. V., and VARANDAS, A. J. C., 1999, *J. chem. Phys.* **111**, 8302.
[37] VARANDAS, A. J. C., 1988, *Adv. chem. Phys.*, **74**, 255.
[38] VARANDAS, A. J. C., 1992, *Chem. Phys. Lett.*, **194**, 333.
[39] ELLISON, F. O., 1963, *J. Am. chem. Soc.*, **85**, 3540.
[40] VARANDAS, A. J. C., and VORONIN, A. I., 1995, *Molec. Phys.*, **95**, 497.
[41] VARANDAS, A. J. C., 1999, Lecture Notes in Chemistry (Berlin: Springer) (to be published).
[42] VARANDAS, A. J. C., BROWN, F. B., MEAD, C. A., TRUHLAR, D. G., and BLAIS, N. C., 1987, *J. chem. Phys.*, **86**, 6258.
[43] VARANDAS, A. J. C., and PAIS, A. A. C. C., 1993, *J. chem. Soc., Faraday Trans.*, **89**, 1511.
[44] PAIS, A. A. C. C., NALEWAJSKI, R. F., and VARANDAS, A. J. C., 1994, *J. chem. Soc., Faraday Trans.*, **90**, 1381.
[45] PASTRANA, M. R., QUINTALES, L. A. M., BRANDÃO, J., and VARANDAS, A. J. C., 1990, *J. phys. Chem.*, **94**, 8073.
[46] VARANDAS, A. J. C., and VORONIN, A. I., 1995, *J. phys. Chem.*, **99**, 15846.
[47] BOGGIO-PASQUA, M., VORONIN, A. I., HALVICK, P., RAYEZ, J. C., and VARANDAS, A. J. C., 1999, *Phys. Chem. chem. Phys.*, (submitted).

[48] Varandas, A. J. C., and Rodrigues, S. P. J., 1997, *J. chem. Phys.*, **106**, 9647.
[49] Varandas, A. J. C., and Pais, A. A. C. C., 1991, *Theoretical and Computational Models for Organic Chemistry*, edited by S. Formosinho, I. Czismadia and L. Arnaut (Dordrecht: Kluwer), p. 55.
[50] Varandas, A. J. C., and Yu, H. G., 1997, *Molec. Phys.*, **91**, 301.
[51] Ishida, T., and Schatz, G. C., 1997, *J. chem. Phys.*, **107**, 3558.
[52] Ishida, T., and Schatz, G. C., 1998, *Chem. Phys. Lett.*, **298**, 285.
[53] Varandas, A. J. C., and Abreu, P. E., 1998, *Chem. Phys. Lett.*, **293**, 261.
[54] Schatz, G. C., 1988, *A. Rev. phys. Chem.*, **39**, 317.
[55] Truhlar, D. G., Schwenke, D. W., and Kouri, D. J., 1990, *J. phys. Chem.*, **94**, 7346.
[56] Miller, W. H., 1990, *A. Rev. phys. Chem.*, **41**, 245.
[57] Ohsaki, A., and Nakamura, H., 1990, *Phys. Rep.*, **187**, 1.
[58] Miller, W. H., 1993, *Accts chem. Res.* **99**, 174.
[59] Bowman, J. M., and Wang, D., 1994, *Advances in Molecular Vibrations and Collision Dynamics*, edited by J. Bowman (Greenwich, Connecticut: JAI Press), p. 187.
[60] Bowman, J. M., and Schatz, G. C., 1995, *A. Rev. phys. Chem.*, **46**, 169.
[61] Clary, D. C., 1994, *J. phys. Chem.*, **98**, 10 678.
[62] Bowman, J. M., 1994, *Advances in Molecular Vibrations and Collision Dynamics: Quantum Reactive Scattering*, Vols 2A and 2B (Greenwich, Connecticut: JAI Press).
[63] Wyatt, R. E., and Zhang, J. Z. H., 1996, *Dynamics of Molecules and Chemical Reactions* (New York: Marcel Dekker).
[64] Szichman, H., and Varandas, A. J. C., and Baer, M., 1994, *Chem. Phys. Lett.*, **231**, 253.
[65] Szichman, H., Varandas, A. J. C., and Baer, M., 1995, *J. chem. Phys.*, **102**, 3474.
[66] Szichman, H., Baer, M., and Varandas, A. J. C., 1997, *J. phys. Chem.*, **101**, 8817.
[67] Szichman, H., Baer, M., and Varandas, A. J. C., 1998, *J. phys. Chem.*, **102**, 8909.
[68] Varandas, A. J. C., and Szichman, H., 1998, *Chem. Phys. Lett.*, **295**, 113.
[69] Szichman, H., and Varandas, A. J. C., 1999, *J. phys. Chem.*, **103**, 1967.
[70] Baer, M., Szichman, H., Rosenman, E., Hochman-Kowal, S., and Persky, A., 1996, *Gas Phase Chemical Reaction Systems*, Springer Series in Chemical Physics, Vol. 61, edited by J. Wolfrum, H.-R. Volpp, R. Rannacher and J. Warnatz (Berlin: Springer).
[71] Varandas, A. J. C., Tennyson, J., and Murrell, J. N., 1979, *Chem. Phys. Lett.*, **61**, 431.
[72] Kendrick, B. K., and Pack, R., 1995, *J. chem. Phys.*, **102**, 1994.
[73] Herzberg, G., and Longuet-Higgins, H. C., 1963, *Discuss. Faraday Soc.*, **35**, 77.
[74] Mead, C. A., and Truhlar, D. G., 1979, *J. chem. Phys.*, **70**, 2284.
[75] Berry, M. V., 1984, *Proc. R. Soc.* A, **392**, 45.
[76] Varandas, A. J. C., Rodrigues, S. P. J., and Gomes, P. A. J., 1998, *Chem. Phys. Lett.*, **297**, 458.
[77] Varandas, A. J. C., 1996, *J. chem. Phys.*, **105**, 3524.
[78] Varandas, A. J. C., 1997, *J. chem. Phys.*, **107**, 867.
[79] Kuntz, P. J., 1979, *Atom–Molecule Collision Theory*, edited by R. Bernstein (New York: Plenum), p. 79.
[80] Tully, J. C., 1980, *Adv. chem. Phys.*, **42**, 63.
[81] Varandas, A. J. C., 1985, *J. molec. Struct. Theochem.*, **120**, 401.
[82] Varandas, A. J. C., 1990, *Trends in Atomic and Molecular Physics*, edited by M. Yáñez (Universidad Autonoma de Madrid), p. 113.
[83] Murrell, J. N., Carter, S., Farantos, S. C., Huxley, P., and Varandas, A. J. C., 1984, *Molecular Potential Energy Functions* (Chichester, West Sussex: Wiley).
[84] Lynch, G., Steckler, R., Schwenke, D. W., Varandas, A. J. C., Truhlar, D. G., and Garrett, B. C., 1991, *J. chem. Phys.*, **91**, 7136.
[85] Varandas, A. J. C., 1987, *Structure and Dynamics of Weakly Bound Molecular Complexes*, edited by A. Weber (Dordrecht: Reidel), p. 357.
[86] Varandas, A. J. C., and Pais, A. A. C. C., 1988, *Molec. Phys.*, **65**, 843.
[87] Boggio-Pasqua, M., Voronin, A. I., Halvick, P., and Rayez, J. C., 1999, *J. molec. Struct. Theochem.* (submitted).
[88] Varandas, A. J. C., 1987, *Int. J. quant. Chem.*, **32**, 563.
[89] Varandas, A. J. C., Voronin, A. I., and Caridade, P. J. S. B., 1998, *J. chem. Phys.*, **108**, 7623.
[90] Prosmiti, R., Polyansky, O. L., and Tennyson, J., 1997, *Chem. Phys. Lett.*, **273**, 107.

[91] HASE, W. L., DUCHOVIC, R. J., HU, X., KOMORNICKI, A., LIM, K. F., LU, D., PESLHERBE, G. H., SWAMY, K. N., LINDE, S. R. V., VARANDAS, A. J. C., WANG, H., and WOLF, R. J., 1996, *QCPE Bull.*, (16), 43.
[92] PORTER, R. N., and RAFF, L. M., 1976, *Modern Theoretical Chemistry, Dynamics of Molecular Collisions*, Part B, Vol. II, edited by W. Miller (New York: Plenum), p. 1.
[93] MAYNE, H., 1996, *Dynamics of Molecules and Chemical Reactions*, edited by R. E. Wyatt and J. Z. H. Zhang (New York: Marcel Dekker), p. 589.
[94] ZHANG, J. Z. H., and MILLER, W. H., 1988, *Chem. Phys. Lett.*, **153**, 465.
[95] ZHANG, J. Z. H., and MILLER, W. H., 1989, *Chem. Phys. Lett.*, **159**, 130.
[96] ZHANG, J. Z. H., and MILLER, W. H., 1989, *J. chem. Phys.*, **91**, 1528.
[97] MIELKE, S. L., LYNCH, G. C., TRUHLAR, D. G., and SCHWENKE, D. W., 1994, *J. phys. Chem.*, **98**, 8000.
[98] BAÑARES, L., AOIZ, F. J., HERRERO, V. J., D'MELLO, M. J., NIEDERJOHANN, B., SEEKAMP-RAHN, K., WREDE, E., and SCHNIEDER, L., 1998, *J. chem. Phys.*, **108**, 6160.
[99] GILIBERT, M., and BAER, M., 1994, *J. phys. Chem.*, **98**, 12822.
[100] ROSENMAN, E., HOCHMAN-KOWAL, S., PERSKY, A., and BAER, M., 1996, *Chem. Phys. Lett.*, **257**, 421.
[101] ROSENMAN, E., PERSKY, A., and BAER, M., 1996, *Chem. Phys. Lett.*, **258**, 639.
[102] CASTILLO, J. F., HARTKE, B., WERNER, H., AOIZ, F. J., BAÑARES, L., and MARTÍNEZ-HAYA, B., 1998, *J. chem. Phys.*, **109**, 7224.
[103] BAER, M., FAUBEL, M., MARTÍNEZ-HAYA, B., RUSIN, L. Y., TAPPE, U., and TOENNIES, J. P., 1998, *J. chem. Phys.*, **108**, 9694.
[104] HAUG, K., SCHWENKE, D. W., TRUHLAR, D. W., ZHANG, Y., ZHANG, J. Z. H., and KOURI, D., 1987, *J. chem. Phys.*, **87**, 1892.
[105] TAKADA, S., TSUDA, K., OHSAKI, A., and NAKAMURA, H., 1994, *Advances in Molecular Vibrations and Collision Dynamics*, edited by J. Bowman (Greenwich, Connecticut: JAI Press), p. 245.
[106] BAER, M., LAST, I., and LOESCH, H.-J., 1994, *J. chem. Phys.*, **101**, 9648.
[107] MANTHE, U., SEIDEMAN, T., and MILLER, W. H., 1994, *J. chem. Phys.*, **101**, 4759.
[108] NEUHAUSER, D., 1994, *J. chem. Phys.*, **100**, 9272.
[109] ZHANG, D. H., and ZHANG, J. Z. H., 1994, *J. chem. Phys.*, **100**, 2697.
[110] ZHANG, D. H., and LIGHT, J. C., 1996, *J. chem. Phys.*, **104**, 4544.
[111] ZHU, W., ZHANG, J. Z. H., ZHANG, Y. C., ZHANG, Y. B., ZHANG, L. X., and ZHANG, D. H., 1998, *J. chem. Phys.*, **108**, 3509.
[112] ZHU, W., ZHANG, J. Z. H., and ZHANG, D. H., 1998, *Chem. Phys. Lett.*, **292**, 46.
[113] BAER, M., and NG, C. Y., 1990, *J. chem. Phys.*, **93**, 7787.
[114] CLARY, D. C., 1992, *J. chem. Phys.*, **96**, 3656.
[115] BALAKRISHNAN, N., and BILLING, G. D., 1994, *J. chem. Phys.*, **189**, 2785.
[116] NEUHAUSER, D., and BAER, M., 1989, *J. chem. Phys.*, **90**, 4351.
[117] ARTHURS, A. M., and DALGARNO, A., 1960, *Proc. R. Soc.*, **256**, 540.
[118] ZHANG, J. Z. H., KOURI, D. J., HAUG, K., SCHWENKE, D. W., SHIMA, Y., and TRUHLAR, D. G., 1988, *J. chem. Phys.*, **88**, 2492.
[119] BAER, M., NEUHAUSER, D., and OREG, Y., 1990, *J. chem. Soc., Faraday Trans.*, **86**, 1721.
[120] SZICHMAN, H., and BAER, M., 1994, *J. chem. Phys.*, **101**, 2081.
[121] MCGUIRE, P., and KOURI, D. J., 1974, *J. chem. Phys.*, **60**, 2488.
[122] PACK, R., 1974, *J. chem. Phys.*, **60**, 633.
[123] MURRELL, J. N., SORBIE, K. S., and VARANDAS, A. J. C., 1976, *Molec. Phys.*, **32**, 1359.
[124] SZICHMAN, H., and BAER, M., 1995, *Chem. Phys. Lett.*, **242**, 285.
[125] YU, H. G., and VARANDAS, A. J. C., 1997, *J. chem. Soc., Faraday Trans.*, **93**, 2651.
[126] SZICHMAN, H., LAST, I., BARAM, A., and BAER, M., 1993, *J. phys. Chem.*, **97**, 6436.
[127] LAST, I., BARAM, A., SZICHMAN, H., and BAER, M., 1993, *J. phys. Chem.*, **97**, 7040.
[128] VARANDAS, A. J. C., 1993, *Dynamical Processes in Molecular Physics*, edited by G. Delgado-Barrio (Bristol: Institute of Physics), p. 3.
[129] MACK, J. A., HUANG, Y., WODTKE, A. M., and SCHATZ, G. C., 1997, *J. chem. Phys.*, **105**, 7495.
[130] LAUVERGNAT, D., and CLARY, D., 1998, *J. chem. Phys.*, **108**, 3566.
[131] MCCRUMB, J. L., and KAUFMAN, F., 1972, *J. chem. Phys.*, **57**, 1270.
[132] DAVIS, D. D., WONG, W., and LEPHARDT, J., 1973, *Chem. Phys. Lett.*, **22**, 273.

[133] West, G. A., Weston, R. E., and Flynn, G. W., 1978, *Chem. Phys. Lett.*, **56**, 429.
[134] Wine, P. H., Nicovich, J. M., Thompson, R. J., and Ravishankara, A. R., 1983, *J. phys. Chem.*, **87**, 3948.
[135] Atkinson, R., Baulch, D. L., Cox, R. A., Hampson, R. F., Jr, Kerr, J. A., and Troe, J., 1992, *J. phys. Chem. Ref. Data*, **21**, 1125.
[136] Houston, P. L., 1995, *Accts chem. Res.*, **28**, 453.
[137] Syage, J. A., 1995, *J. phys. Chem.*, **99**, 16530.
[138] Stranges, D., Yang, X. M., Chesko, J. D., and Suits, A. G., 1995, *J. chem. Phys.*, **102**, 6067.
[139] Toumi, R., Houston, P. L., and Wodtke, A. M., 1996, *J. chem. Phys.*, **104**, 775.
[140] Varandas, A. J. C., and Wang, W., 1997, *Chem. Phys.*, **215**, 167.
[141] Wang, W., and Varandas, A. J. C., 1998, *Chem. Phys.*, **236**, 181.
[142] Balakrishnan, N., and Billing, G. D., 1995, *Chem. Phys. Lett.*, **242**, 68.
[143] Hernández-Lamoneda, R., Hernández, M. I., Carmona-Novillo, E., Campos-Martínez, J., Echave, J., and Clary, D. C., 1997, *Chem. Phys. Lett.*, **276**, 152.
[144] Campos-Martínez, J., Carmona-Novillo, E., Echave, J., Hernández, M. I., Hernández-Lamoneda, R., and Palma, J., 1998, *Chem. Phys. Lett.*, **289**, 150.
[145] Yang, X., Price, J. M., Mack, J. A., Morgan, C. G., Rogaski, C. A., McGuire, D., Kim, E. H., and Wodtke, A. M., 1993, *J. phys. Chem.*, **93**, 3944.
[146] Rogaski, C. A., Mack, J. A., and Wodtke, A. M., 1995, *Faraday Discuss. atmos. Chem.*, **100**, 229.
[147] Blint, R. J., and Newton, M. D., 1973, *J. chem. Phys.*, **59**, 6220.
[148] Mathisen, K. B., Gropen, O., Skancke, P. N., and Wahlgren, U., 1983, *Acta chem. Scand.* A, **37**, 817.
[149] Mathisen, K. B., and Siegbahn, P. E. M., 1984, *Chem. Phys.*, **90**, 225.
[150] Chen, M. M. L., Wetmore, R. W., and Schaefer, H. F., III, 1981, *J. chem. Phys.*, **74**, 2938.
[151] Dupuis, M., Fitzgerald, G., Hammond, B., Lester, W. A., Jr, and Schaefer, H. F., III, 1986, *J. chem. Phys.*, **84**, 2691.
[152] Vincent, M. A., and Hillier, I. H., 1995, *J. phys. Chem.*, **99**, 3109.
[153] Jungkamp, T. P. W., and Steinfeld, J. H., 1996, *Chem. Phys. Lett.*, **257**, 15.
[154] Speranza, M., 1996, *Inorg. Chem.*, **35**, 6140.
[155] Speranza, M., 1998, *J. phys. Chem.*, **102**, 7535.
[156] LeRoy, R. L., 1969, *J. chem. Phys.*, **73**, 4338.
[157] Phillips, L. F., and Schiff, H. I., 1962, *J. chem. Phys.*, **37**, 1233.
[158] Baulch, D. L., Cox, R. A., Crutzen, P. J., Hampson, R. F., Jr, Kerr, J. A., Troe, J., and Watson, R. T., 1982, *J. phys. Chem. Ref. Data*, **11**, 327.
[159] Clyne, M. A. A., and Monkhouse, P. B., 1977, *J. chem. Soc., Faraday Trans. II*, **73**, 298.
[160] Lee, J. H., Michael, J. V., Payne, W. A., and Stief, L. J., 1978, *J. chem. Phys.*, **69**, 350.
[161] Keyser, L. F., 1979, *J. phys. Chem.*, **83**, 645.
[162] Greenblatt, G. D., and Wiesenfeld, J. R., 1982, *J. geophys. Res.*, **87**, 11145.
[163] Wang, W., González-Jonte, R., and Varandas, A. J. C., 1998, *J. phys. Chem.*, **102**, 6935.
[164] Weisman, M., Shum, L. S. G., Heneghan, S. P., and Benson, S. W., 1981, *J. phys. Chem.*, **85**, 2863.
[165] Sridharan, U. C., Qiu, L. X., and Kaufman, F., 1982, *J. phys. Chem.*, **86**, 4469.
[166] Ravishankara, A. R., Wine, P. H., and Nicovich, B. M., 1983, *J. chem. Phys.*, **78**, 6629.
[167] Nicovich, J. M., and Wine, P. H., 1987, *J. phys. Chem.*, **91**, 5118.
[168] Sridharan, U. C., Klein, F. S., and Kaufman, F., 1985, *J. chem. Phys.*, **82**, 592.
[169] Clary, D. C., 1992, *Chem. Phys. Lett.*, **192**, 34.
[170] Wang, D., and Bowman, J. M., 1993, *Chem. Phys. Lett.*, **207**, 227.
[171] Langhoff, S. R., and Jaffe, R. L., 1979, *J. chem. Phys.*, **71**, 1475.
[172] Johnson, B. R., and Winter, N. W., 1977, *J. chem. Phys.*, **66**, 4116.
[173] Keyser, L. F., 1982, *J. phys. Chem.*, **86**, 3439.
[174] Hack, W., Preuss, A. W., Temps, F., and Wagner, H., 1979, *Ber. Bunsenges. phys. Chem.*, **83**, 1275.
[175] Brune, W. H., Schwab, J. J., and Anderson, J. G., 1983, *J. phys. Chem.*, **87**, 4503.
[176] Lii, R. R., Sauer, M. C., and Gordon, S., 1980, *J. phys. Chem.*, **84**, 817.

[177] PEETERS, J., and MAHNEN, G., 1973, *Proceedings of the 14th International Symposium on Combustion*, 1972 (Pittsburgh Pennsylvania: Combustion Institute), p. 133.
[178] DAY, M. J., THOMPSON, K., and DIXON-LEWIS, G., 1973, *Proceedings of the 14th International Symposium on Combustion*, 1972 (Pittsburgh Pennsylvania: Combustion Institute), p. 47.
[179] GARRIDO, J. D., CARIDADE, P. J. S. B., and VARANDAS, A. J. C., 1999, *J. phys. Chem.*, **103**, 4815.
[180] VARANDAS, A. J. C., 1987, *Discuss. Faraday Soc.*, **84**, 353.
[181] RODRIGUES, S. P. J., and VARANDAS, A. J. C., 1998, *J. phys. Chem.*, **102**, 6266.
[182] CLARY, D. C., DATEO, C. E., and STOECKLIN, T., 1990, *J. chem. Phys.*, **93**, 7666.
[183] VARANDAS, A. J. C., 1987, *Molec. Phys.*, **60**, 527.
[184] COOKSY, A. L., DRUCKER, S., FAEDER, J., GOTTLIEB, C. A., and KLEMPERER, W., 1991, *J. chem. Phys.*, **95**, 3017.
[185] DRUCKER, S., COOKSY, A. L., and KLEMPERER, W., 1993, *J. chem. Phys.*, **98**, 5158.
[186] HOLBROOK, K. A., PILLING, M. J., and ROBERTSON, S. H., 1996, *Unimolecular Reactions* (Chichester, West Sussex: Wiley).
[187] HERZBERG, G., 1966, *Molecular Spectra and Molecular Structure*. III. *Electronic Spectra and Electronic Structure of Polyatomic Molecules* (New York: Van Nostrand).
[188] TABAYASHI, K., FUENO, T., TAKASA, K., KAJIMOTO, O., and OKADA, K., 1977, *Bull. chem. Soc. Japan*, **50**, 1754.
[189] ROTH, P., and JUST, T., 1976, *Ber. Bunsenges. phys. Chem.*, **80**, 171.
[190] SZEKELY, A., HANSON, R. K., and BOWMAN, C. T., 1984, *J. phys. Chem.*, **88**, 666.
[191] SZEKELY, A., HANSON, R., and BOWMAN, C. T., 1982, *Proceedings of the 13th Symposium on Shock Tubes and Waves*, edited by C. Treanor and J. Hall (State University of New York Press), p. 617.
[192] KIEFER, J. H., MUDIPALLI, P. S., WAGNER, A. F., and HARDING, L., 1996, *J. chem. Phys.*, **105**, 8075.
[193] CARIDADE, P. J. S. B., ZHANG, L., GARRIDO, J. D., and VARANDAS, A. J. C., to be published.
[194] VARANDAS, A. J. C., and ZHANG, L., preliminary results.